

ENTANGLEMENT AND THERMAL TRANSITIONS FROM SINGULARITIES

Sergio Barbosa^{a *}, Sylvain Fichet^{a †}, Eugenio Megías^{b ‡}, Mariano Quirós^{c §}

^a *Centro de Ciências Naturais e Humanas, Universidade Federal do ABC,
Santo André, 09210-580 SP, Brazil*

^b *Departamento de Física Atómica, Molecular y Nuclear and
Instituto Carlos I de Física Teórica y Computacional,
Universidad de Granada, Avenida de Fuente Nueva s/n, 18071 Granada, Spain*

^c *Institut de Física d'Altes Energies (IFAE) and
The Barcelona Institute of Science and Technology (BIST),
Campus UAB, 08193 Bellaterra, Barcelona, Spain*

Abstract

We study holographic entanglement entropy and revisit thermodynamics and confinement in the dilaton-gravity system. Our analysis focuses on a solvable class of backgrounds that includes AdS and linear dilaton spacetimes as particular cases, with some results extended to general warped metrics. A general lesson is that the behavior of the holographic theory is tied to the bulk curvature singularities. We find that a singular background is confining if and only if *i*) the singularity coincides with a boundary or *ii*) it is the linear dilaton. In the former case, for which the singularity cuts off spacetime, we demonstrate that both entanglement entropy and thermodynamics exhibit a first order phase transition. In the linear dilaton case we find instead that both entanglement entropy and thermal phase transitions are of second order. Additionally, along the process we thoroughly derive the radion effective action at quadratic order.

*sergio.barbosa@ufabc.edu.br

†sylvain.fichet@gmail.com

‡emegias@ugr.es

§quiros@ifae.es

Contents

1	Introduction	3
2	Dilaton-Gravity and Singularities	4
2.1	The \mathcal{M}_ν spacetime	5
2.2	The Black Hole	5
2.3	On Singularities and Boundaries	5
3	Holographic Confinement	7
3.1	The Holographic Wilson Loop	7
3.2	String Shape in Dilatonic Background	8
3.3	Confinement	10
3.4	Comparison to Asymptotically AdS backgrounds	11
4	Spacelike Geodesics	12
4.1	Geodesics of \mathcal{M}_ν^- with no Black Hole	12
4.2	Geodesics of \mathcal{M}_ν^- with a Black Hole	14
4.3	Geodesics in Linear Dilaton Spacetime	15
5	Holographic Entanglement Entropy	16
5.1	Elementary Properties	16
5.2	Phase Transition and Boundaries	18
5.3	Holographic Entanglement Entropy in the \mathcal{M}_ν^- background	20
6	Stability and the Radion Effective Action	22
6.1	The Effective Potential	22
6.2	The Radion	22
6.3	Radion Mass from the On-Shell Action	24
7	Holographic Thermal Phase Transitions	25
7.1	Thermodynamics on the Brane	26
7.2	Phase Transitions	27
7.3	Discussion	29
7.4	Instability from Big Black Holes	30
8	Summary	31
A	Derivation of Property (2.10)	34
B	Geodesic Distances	35
B.1	Anti-de Sitter Spacetime	35
B.2	\mathcal{M}_ν^- Spacetime with No Black Hole	36
B.3	\mathcal{M}_ν^- Spacetime with a Black Hole	36

1 Introduction

The phenomenon of confinement remains an unsolved puzzle of QFT at strong coupling. One route to understand confinement is to describe it holographically, using a gauge-gravity duality that may potentially encode the strong dynamics in a gravitational higher-dimensional spacetime. While the most precise and well-established duality of this kind is the AdS/CFT correspondence [1–4], CFTs cannot confine since they have no scale. The holographic view of confinement, if it exists, must come from a different, less symmetric spacetime beyond AdS, that allows for the emergence of a confinement scale.

The gauge-gravity correspondence being an offspring of string theory, natural candidates for holography beyond AdS are motivated by non-critical string-inspired models [5–9]. The low-energy effective action in such models describes spacetime augmented with an extra scalar field, the dilaton. Going beyond AdS/CFT naturally leads to exploring the properties of the dilaton-gravity system.

One reason to expect that dilatonic backgrounds are holographic is the existence of a known example: the linear dilaton spacetime, whose corresponding dual theory is little string theory (LST).⁴ More generally it is widely accepted that a (less predictive) holographic principle formulated in terms of information content applies to any spacetime [36–40]. These are strong motivations to investigate the holography of the dilaton-gravity system, including the holographic version of confinement.⁵

Hints that certain non-AdS spacetime backgrounds describe confining dynamics have been gradually gathered, using holographic descriptions of the quark-antiquark potential [9, 47–55], of thermal phase transitions [56–63], and of entanglement entropy [64–75]. Such phenomena can be viewed as probes that test whether a background is confining, based on the broad qualitative features expected from confining theories.

While a number of studies of holographic entanglement entropy — as a probe of confinement — have been done in stringy and supersymmetric backgrounds (see [64–73, 75–79]), holographic entanglement has not been studied in the simple dilaton-gravity system, to the best of our knowledge, apart from a brief case study [80]. One goal of this paper is to fill this important gap.

Another objective of this study is to elucidate the relationship between curvature singularities and confinement. These singularities, induced by the backreaction of the metric on the dilaton vacuum expectation value (vev), are prevalent in dilaton-gravity models. Here, we will categorize the singularities in terms of conformal distance to the brane, a distinction that we will show to be linked to the confining nature of the background.

A third objective of this paper is to provide a unified view and a simple set of intuitions for the various probes of confinement, that can be applied to e.g. asymptotically AdS backgrounds. Here we compute all these phenomena in a class of non-asymptotically AdS backgrounds (first introduced in [81]) that retains the essence of the features we want to

⁴See [10–12] for LST reviews, [13–27] for formal holographic aspects of the linear dilaton background, and [12, 28–35] for field theoretical studies of the LD background and related phenomenological developments.

⁵See e.g. [8, 9, 41–46] for related studies of the dilaton-gravity system.

highlight. This class of backgrounds has a single continuous parameter and contains both the linear dilaton and AdS as particular cases.

Our study is structured as follows. In section 2 we define the D -dimensional dilaton-gravity system of our interest, and classify its curvature singularities. In section 3 we analyze the string-based notion of confinement in this background, developing intuitions that also apply to asymptotically-AdS backgrounds. In section 4 we compute and discuss the spacelike geodesics in our class of dilatonic spacetimes. We then compute in section 5 the holographic entanglement entropy of a $(D-2)$ -strip localized on the boundary, including finite temperature corrections. In section 6 we compute the radion effective action. At zero temperature this provides the stability of the brane-dilaton system. At finite temperature the radion effective action gives access to the free energy. We explore the structure of phase transitions in section 7. Our findings are summarized in section 8. The Appendix contains a derivation of a property used in the analysis of metric zeros (A) and details on the geodesics computation (B).

2 Dilaton-Gravity and Singularities

We consider a spacetime with $D = d + 1$ dimensions. The action of the D -dimensional dilaton-gravity system in the Einstein frame is

$$\begin{aligned} \mathcal{S} = & \int d^D x \sqrt{g} \left(\frac{M_D^{D-2}}{2} {}^{(D)}R - \frac{1}{2} (\partial_M \phi)^2 - V(\phi) \right) \\ & - \int_{\text{brane}} d^d x \sqrt{\bar{g}} \left(V_b(\phi) + \Lambda_b - M_D^{D-2} K \right) + \mathcal{S}_{\text{matter}}, \end{aligned} \quad (2.1)$$

where ${}^{(D)}R$ is the scalar curvature, ϕ the dilaton field, M_D the fundamental D -dimensional Planck scale, and g_{MN} the bulk metric with mostly plus signature. The spacetime supports a $(d-1)$ -brane, with induced metric $\bar{g}_{\mu\nu}$, tension Λ_b and a localized potential $V_b(\phi)$. K is the extrinsic curvature that appears in the Gibbons-Hawking-York (GHY) boundary term. The $V_b(\phi)$ potential stabilizes ϕ to the vacuum expectation value (vev) $\langle \phi \rangle_{\text{brane}} \equiv v_b$, which determines completely the background. $\mathcal{S}_{\text{matter}}$ encodes the quantum fields living on this background.

The $V_b(\phi)$ potential does not need to be explicitly specified. We use the convention $V_b(v_b) = 0$ without loss of generality. Conditions on V_b for the stability of spacetime have been derived in [81].

The most general metric ansatz we consider is the warped foliation

$$ds^2 = g_{MN} dx^M dx^N = g_{xx}(r) \eta_{\mu\nu} dx^\mu dx^\nu + g_{rr}(r) dr^2 \quad (2.2)$$

with arbitrary g_{xx} , g_{rr} coefficients. Some of our results will be derived with this general metric, using sometimes monotonicity assumptions involving the metric coefficients.

2.1 The \mathcal{M}_ν spacetime

We introduce the reduced bulk potential $V(\phi) \equiv (D-2)M_D^{D-2}\bar{V}(\bar{\phi})$ and the reduced dilaton field $\phi \equiv \sqrt{(D-2)M_D^{D-2}}\bar{\phi}$. \bar{V} has mass dimension 2, while $\bar{\phi}$ is dimensionless. The \mathcal{M}_ν spacetime used in this work is defined by setting the reduced bulk potential to

$$\bar{V}(\bar{\phi}) = -\frac{1}{2}(D-1-\nu^2)k^2 e^{2\nu\bar{\phi}}. \quad (2.3)$$

Here ν is a real parameter that we take positive without loss of generality.

In the absence of a black hole horizon, the solutions to the field equations following from the action (2.1) are found to be [81]

$$ds_{\nu,r_b}^2 = \left(\frac{r}{L}\right)^2 \eta_{\mu\nu} dx^\mu dx^\nu + \left(\frac{r}{r_b}\right)^{2\nu^2} \frac{1}{(\eta r)^2} dr^2, \quad (2.4)$$

$$\bar{\phi}(r) = \bar{\phi}_b - \nu \log\left(\frac{r}{r_b}\right), \quad (2.5)$$

with $r \in \mathbb{R}_+$. L is a constant with dimension of length. In (2.5), $\bar{\phi}_b = \frac{1}{\sqrt{(D-2)M_D^{D-2}}}\phi_b$ is the value of the reduced dilaton field on the brane, with $\phi_{\text{brane}} \equiv \phi_b$. The value of ϕ_b is stabilized to the vev $\langle\phi_b\rangle = v_b$ due to the brane-localized potential. The dilaton vev and the other parameters of the metric combine to form the physical scale $\eta \equiv k e^{\nu\bar{v}_b}$ that appears in observable quantities.

The brane at $r = r_b$ partitions \mathcal{M}_ν into two regions

$$\mathcal{M}_\nu^- = \mathcal{M}_\nu|_{r \in (0, r_b]}, \quad \mathcal{M}_\nu^+ = \mathcal{M}_\nu|_{r \in [r_b, \infty)}. \quad (2.6)$$

Our focus in this work is the \mathcal{M}_ν^- space. We mention sometimes \mathcal{M}_ν^+ for comparison.

2.2 The Black Hole

Extending the result from [81], the \mathcal{M}_ν^- spacetime admits a planar black hole solution:⁶

$$ds_{\nu,r_b}^2 = \left(\frac{r}{L}\right)^2 (-f(r)d\tau^2 + d\mathbf{x}^2) + \frac{1}{f(r)} \left(\frac{r}{r_b}\right)^{2\nu^2} \frac{1}{(\eta r)^2} dr^2, \quad (2.7)$$

with the blackening factor

$$f(r) = 1 - \left(\frac{r_h}{r}\right)^{D-1-\nu^2}, \quad (2.8)$$

where r_h is the location of the horizon.

2.3 On Singularities and Boundaries

For clarity, throughout this work, we refer to a boundary as *a regular boundary*, to emphasize the distinction with the notion of conformal boundary. In the vicinity of a regular

⁶The black hole in the 4D linear dilaton case was independently found in [82].

boundary, spacetime is isomorphic to the half flat space. A conformal boundary is similarly defined, but up to a suitable Weyl rescaling to Minkowski space.

2.3.1 Metric Zeros and Singularities

We show how zeros of the metric are related to divergences of the curvature. We go to conformal coordinates denoted (x^μ, z) for which the coefficients of the general metric (4.1) are $g_{xx}(z) = g_{zz}(z) \equiv a(z)$. The curvature scalar is

$$R = -(D-1) \frac{(D-6)(a')^2 + 4aa''}{4a^3}, \quad (2.9)$$

where the prime ($'$) denotes derivative with respect to z .

We assume that the scale factor $a(z)$ goes to zero at a *finite* value z_s . Assuming that z_s is approached from above, we have $\lim_{z \rightarrow z_s^+} \frac{1}{a(z)} = \infty$. We then use the following property:

If $a(z)$ vanishes at finite z_s , then : $\lim_{z \rightarrow z_s^+} \frac{a'(z)}{a(z)} = \infty$.

(2.10)

This property is shown in App. A using the mean value theorem — with the mild assumption that $\frac{a'(z)}{a(z)}$ is strictly monotonous in the vicinity of the singularity. Using the definition of the curvature (4.1), (2.10) implies that $\lim_{z \rightarrow z_s^+} R(z) = \infty$. That is, the scalar curvature diverges at z_s . Summarizing:

If there is a conformal coordinate $z_s < \infty$ for which the scale factor satisfies $a(z_s) = 0$, then there is a curvature singularity at z_s .

(2.11)

We emphasize that the assumption of *finite* z_s is key for the proof. If $z_s = \infty$, the mean value theorem does not apply, and thus Prop. (2.10) does not hold. As an example of non-applicability, AdS space in conformal coordinates $a(z) \propto z^{-2}$, for which $z_s = \infty$, has $a(z_s) = 0$, yet it has finite R at z_s since R is constant everywhere.

Finally, when a singularity appears, the general relativity description breaks down and we must cut off spacetime. In our case we have to require that $z > z_s$, which is a regular boundary. In other words, the metric zero describes a singularity that truncates spacetime.

2.3.2 The \mathcal{M}_ν spacetime case

We summarize the structure of boundaries and singularities of the \mathcal{M}_ν spacetime, bearing in mind the general discussion of Sec. 2.3.1.

In \mathcal{M}_ν , the scalar curvature diverges at $r \rightarrow 0$ for any $\nu > 0$. There is thus a curvature singularity at $r = 0$, which lies in the \mathcal{M}_ν^- part of the spacetime. The singularity is labeled as “good” in the sense of Refs. [44, 83] if $\nu < 2$. This is confirmed by [81] where it is found that $\nu \in [0, 2)$ is the range of values for which the singularity can get censored by a black hole horizon. The \mathcal{M}_ν^+ spacetime does not feature any singularity for any ν .

We now go to conformal coordinates to analyze boundaries, for which $a(z) \propto z^{\frac{2}{\nu^2-1}}$, see [81] for details. For $\nu < 1$ there is a conformal timelike boundary, however it belongs to \mathcal{M}_ν^+ . For $\nu > 1$ there is a regular boundary at $z = 0$. In the special case of $\nu = 1$ (linear dilaton) the boundaries are null, the Penrose diagram is the same as Minkowski, and the singularity is at a spatial infinity of the causal diamond.

We can see that Prop. (2.11) applies. For $\nu > 1$, we have $a(z_s) = 0$ at a finite conformal distance $z_s = 0$. Using (2.11) we conclude that there is a curvature singularity there, that coincides with the regular boundary. That is, the singularity cuts off space to $z > 0$. For $\nu \leq 1$, we have instead $z_s = \infty$. In that case Prop. (2.11) does not apply: there is a singularity for $\nu > 0$ but not when $\nu = 0$ (AdS case).

3 Holographic Confinement

We classify the \mathcal{M}_ν^- dilaton gravity backgrounds in terms of confinement. In the holographic view of confinement, a Wilson loop on the boundary is evaluated as a string extending into the bulk⁷. The background is said to be *confining* if the Wilson loop features an area law, i.e. if the corresponding $q\bar{q}$ potential grows linearly with $q\bar{q}$ separation. In the \mathcal{M}_ν^- dilaton gravity background considered here, the string is attached to the brane located at $r = r_b$.

3.1 The Holographic Wilson Loop

We review the holographic computation of the quark-antiquark potential, here generalized to any bulk dimension. The potential energy $V(\ell)$ of a static $q\bar{q}$ pair separated by a distance ℓ is conjectured to be computed in the bulk by

$$TV(\ell) \equiv S_{\text{NG}}[x_{\text{cl}}^M(\sigma, \tau)]. \quad (3.1)$$

S_{NG} is the Nambu-Goto action, $x^M(\sigma, \tau)$ is the worldsheet embedding for the string attached to a rectangle of size (T, ℓ) on the brane, and $x_{\text{cl}}^M(\sigma, \tau)$ describes the string configuration of minimal surface, that we refer to as the classical configuration. The Nambu-Goto action in (3.1) is “on-shell” in the sense that it is evaluated on the classical configuration.

We have

$$S_{\text{NG}}[x^M(\sigma, \tau)] = T_f \int d\tau d\sigma \sqrt{\det(-\hat{g}_s)} \quad (3.2)$$

where \hat{g}_s denotes the induced metric on the worldsheet, and T_f is the string tension. The worldsheet embedding $x^M(\sigma, \tau)$ defines the D -dimensional string frame metric $(g_s)_{MN}$ as

$$(\hat{g}_s)_{\alpha\beta} = (g_s)_{MN} \partial_\alpha x^M \partial_\beta x^N. \quad (3.3)$$

Assuming that the string frame metric takes the diagonal form

$$ds_s^2 = -g_{s,00} dt^2 + g_{s,rr} dr^2 + g_{s,ii} dx_i^2, \quad (3.4)$$

⁷See e.g. [47–52, 84] for seminal papers and [9] for a detailed study in holographic QCD. Here we mostly use [9, 84].

choosing worldsheet coordinates $\tau = t$, $\sigma = x^1 \equiv x$, and assuming invariance in time, one obtains [84]

$$S_{\text{NG}}[x^M(\sigma, \tau)] = T_f \int dx \sqrt{h^2(r) + k^2(r)r'^2}, \quad (3.5)$$

with

$$h^2(r) = g_{s,00}(r)g_{s,ii}(r), \quad k^2(r) = g_{s,00}(r)g_{s,rr}(r), \quad (3.6)$$

and $r' \equiv \frac{dr}{dx}$. The classical solution, i.e. the configuration of minimal length, is denoted by $r_{\text{cl}}(x)$.

Assuming no restriction on the domain of coordinates, the string geodesic equation that determines $r_{\text{cl}}(x)$ can be readily deduced from Eq. (3.5),

$$\frac{dr}{dx} = \pm \frac{h(r)}{k(r)} \frac{\sqrt{h^2(r) - h_0^2}}{h_0}, \quad (3.7)$$

with $h_0 = h(r_0)$, where r_0 corresponds to the tip of the geodesic which satisfies $\frac{dr}{dx}|_{r_0} = 0$. h_0 can be considered as a constant of motion that parameterizes the geodesics.

Finally, for a given spacetime background, the string frame metric $(g_s)_{MN}$ is obtained by converting frames in the low-energy effective action. The string and Einstein frames are related in any dimension by use of the conformal rescaling

$$g_{MN} = e^{-2\bar{\phi}} g_{s,MN}, \quad (3.8)$$

where $\bar{\phi} = \frac{\phi}{\sqrt{(D-2)M_D^{D-2}}}$ is the reduced dilaton field introduced in section 2. Starting from the Einstein frame action (2.1), we find the bulk action in string frame

$$\mathcal{S}_s = \frac{M_D^{D-2}}{2} \int d^D x \sqrt{g_s} e^{-(D-2)\bar{\phi}} \left({}^{(D)}R_s + (D-2)^2 (\partial_M \bar{\phi})^2 - \bar{V}_s(\bar{\phi}) \right), \quad (3.9)$$

where $\bar{V}_s = 2(D-2)e^{-2\bar{\phi}}\bar{V}$. The low-energy string effective action in the usual convention from e.g. [85–87] is recovered by normalizing the dilaton field as $\bar{\phi}_s \equiv \frac{D-2}{2}\bar{\phi}$.

3.2 String Shape in Dilatonic Background

We apply the above formalism to our dilatonic background \mathcal{M}_ν with Einstein metric (2.4). The string frame metric and derived quantities are

$$ds_{\nu, r_b, s}^2 = e^{2\bar{\phi}_b} \left(\frac{r_b}{L} \right)^2 \left(\frac{r}{r_b} \right)^{2-2\nu} \eta_{\mu\nu} dx^\mu dx^\nu + e^{2\bar{\phi}_b} \frac{1}{\eta^2 r_b^2} \left(\frac{r}{r_b} \right)^{2\nu^2 - 2\nu - 2} dr^2, \quad (3.10)$$

$$h(r) = e^{2\bar{\phi}_b} \left(\frac{r_b}{L} \right)^2 \left(\frac{r}{r_b} \right)^{2-2\nu}, \quad k(r) = e^{2\bar{\phi}_b} \frac{1}{\eta L} \left(\frac{r}{r_b} \right)^{\nu^2 - 2\nu}. \quad (3.11)$$

We can notice that the metric is Minkowski when $\nu = 1$: the linear dilaton background is flat in the string frame. The reduced potential is $\bar{V}_s = -(D-2)(D-1-\nu^2)k^2 e^{2(\nu-1)\bar{\phi}}$. In the linear dilaton case, \bar{V}_s reduces to a constant, which is consistent with results in the

literature. The value is $\bar{V}_s|_{\nu=1} = -(D-2)^2 k^2$.

To understand the behavior of the string in our dilatonic background, let us consider a static string configuration with endpoints lying at coordinates $(0, \tilde{r})$ and $(\Delta x, \tilde{r})$ in the bulk. In the critical case $\nu = 1$ i.e. the linear dilaton, the classical string configuration simply is the straight line, $r_{\text{cl}}(x) \equiv \tilde{r}$. We establish a useful qualitative property:

$$\boxed{\text{If } \nu < 1 \text{ (} \nu > 1 \text{) the classical string configuration bends towards } r < \tilde{r} \text{ (} r > \tilde{r} \text{).} \quad (3.12)}$$

We show this at the infinitesimal level as follows. We consider the straight line configuration, given by $r(x) \equiv \tilde{r}$ for all x . The corresponding Nambu-Goto action is $\tilde{\mathcal{S}}_{\text{NG}} = T_{\text{f}} \Delta x h(\tilde{r})$. We then consider a small perturbation to the straight line, $r(x) = \tilde{r} + \delta r(x)$, with $\delta r \ll \tilde{r}$ for all x . The action for this perturbed configuration is

$$\mathcal{S}_{\text{NG}} = \tilde{\mathcal{S}}_{\text{NG}} + \delta \mathcal{S}_{\text{NG}}, \quad \delta \mathcal{S}_{\text{NG}} = T_{\text{f}} \int dx (h'(\tilde{r}) \delta r(x) + O(\delta r^2)), \quad (3.13)$$

with $h'(r) = \frac{dh(r)}{dr}$. Let us further assume that the perturbation is towards $r > \tilde{r}$, i.e. $\delta r(x) > 0$ for all x . It follows that

$$\text{sign}(\delta \mathcal{S}_{\text{NG}}) = \text{sign}(h'(\tilde{r})). \quad (3.14)$$

This relation implies that, relative to the straight line configuration, the perturbed configuration has lower (higher) energy if $h'(\tilde{r}) < 0$ ($h'(\tilde{r}) > 0$). Similarly, for $\delta r(x) < 0$ (in which case the perturbation is toward $r < \tilde{r}$) the perturbed configuration has lower energy if $h'(\tilde{r}) > 0$.

Using the explicit expression of h in Eq. (3.11), it follows that, at the infinitesimal level, string configurations with $r < \tilde{r}$ (resp. $r > \tilde{r}$) are favored if $\nu < 1$ (resp. $\nu > 1$). This proves the infinitesimal version of Prop. (3.12).

We can also derive Prop. (3.12) at the finite level by inspecting the classical string configurations. Assuming that the tip of the classical configuration r_0 is inside the spacetime, the classical configuration is determined by the geodesic equation (3.7). We see from this equation that h_0 must be smaller than $h(r_{\text{cl}})$ for all values of r_{cl} . This condition is satisfied in the $r_0 < r_{\text{cl}} < \tilde{r}$ region if h is monotonic increasing, and conversely in the $r_0 > r_{\text{cl}} > \tilde{r}$ region if h is monotonic decreasing. Since h increases if $\nu < 1$, and decreases if $\nu > 1$, we obtain again Prop. (3.12).

Finally, we notice that the scalar curvature in string frame is

$$R_s = -(D-1)(\nu-1)^2 (D+2\nu) e^{-2\bar{v}_b} \eta^2 \left(\frac{r}{r_b} \right)^{2\nu(1-\nu)}. \quad (3.15)$$

Hence the curvature singularity in string frame is at $r \rightarrow \infty$ for $\nu < 1$ and $r = 0$ for $\nu > 1$. Hence qualitatively we can say that, the string living in the \mathcal{M}_ν background is *repelled* by the (string frame) singularity. Accordingly, for $\nu = 1$ we have $R_s = 0$, hence there is no singularity, therefore the string is straight.

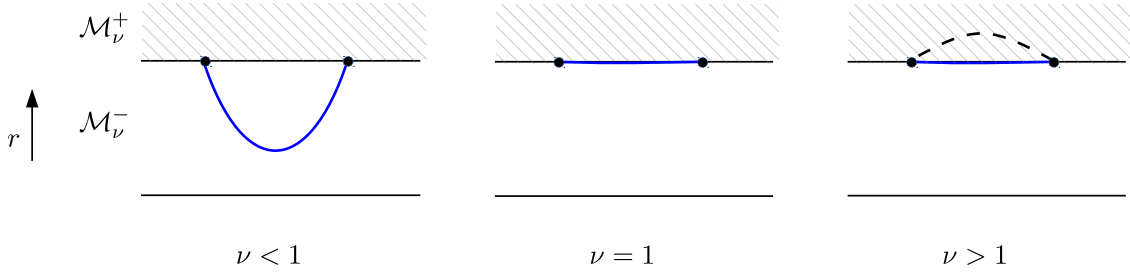


Figure 1. The classical string attached to the brane in the \mathcal{M}_ν^- background. The configuration is a straight line for both $\nu = 1$ (because it is geodesic) and $\nu > 1$ (because it is stuck to the brane). In both cases the background is confining with same string tension $T_s = T_f e^{2\bar{\phi}_b} \left(\frac{r_b}{L}\right)^2$.

3.3 Confinement

We consider the \mathcal{M}_ν^- spacetime, for which $0 < r < r_b$. The string is anchored to the brane at $r = r_b$. The behavior of the classical configuration is obtained using Prop. (3.12).

If $\nu < 1$, the classical string configuration bends towards $r < r_b$. In that case the geodesic equation (3.7) applies. The string length is given by [84]

$$\ell = \int_{\text{cl}} dx = 2 \int_{r_0}^{r_b} dr \frac{k(r)}{h(r)} \frac{h_0}{\sqrt{h^2(r) - h_0^2}}, \quad (3.16)$$

and the potential is given by

$$V(\ell) = T_f \int_{\text{cl}} \mathcal{L} dx = 2T_f \int_{r_0}^{r_b} dr \frac{k(r)}{h(r)} \frac{h^2(r)}{\sqrt{h^2(r) - h_0^2}}. \quad (3.17)$$

The integrals can be done analytically, but the expressions are not particularly enlightening. We find numerically that $V(\ell)$ is not proportional to ℓ for any value of r_0 , except in the $\nu \rightarrow 1$ limit.

If $\nu = 1$, the classical string follows a straight geodesic along $r = r_b$. We find

$$V(\ell) = T_f e^{2\bar{\phi}_b} \left(\frac{r_b}{L}\right)^2 \ell. \quad (3.18)$$

That is, the potential grows linearly with ℓ , for any ℓ . The linear dilaton is therefore a confining background with string tension

$$T_s = T_f e^{2\bar{\phi}_b} \left(\frac{r_b}{L}\right)^2. \quad (3.19)$$

The same result is obtained when taking the $\nu \rightarrow 1$ limit from (3.16) and (3.17).

If $\nu > 1$, the string would bend towards $r > r_b$, however this region does not exist in \mathcal{M}_ν^- . Using (3.12), the allowed configuration of lower energy is the straight line along $r = r_b$. We find again the confining potential Eq. (3.18) because $h(r_b)$ is independent on ν , hence $h(r_b)|_{\nu>1} = h(r_b)|_{\nu=1}$. The string tension is again given by Eq. (3.19). These features are summarized in Fig. 1.

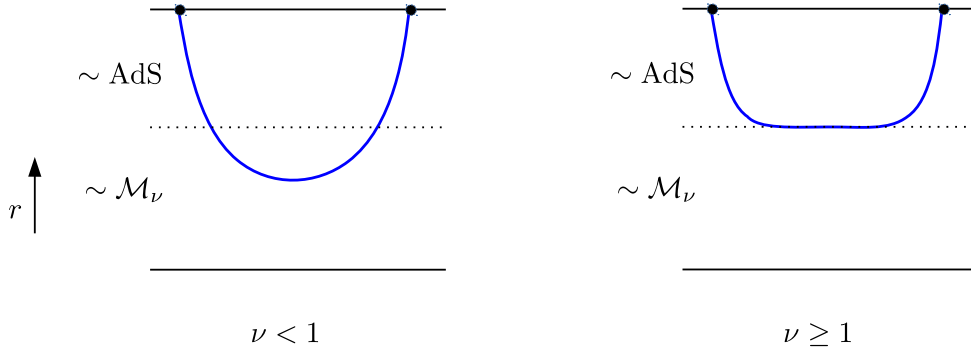


Figure 2. The classical string attached to a brane in an asymptotic AdS background. For $\nu \geq 1$ the string enters the asymptotic \mathcal{M}_ν region only up to a finite value of r . Accordingly it asymptotically follows an area law with tension $T_s = T_s e^{2\bar{\phi}_b} \left(\frac{r_b}{L}\right)^2$.

In terms of the curvature singularity in string frame, we can say that confinement occurs if the singularity is in \mathcal{M}_ν^- , such as the string is repelled as shown in the $\nu > 1$ case of Fig. 1, or if it is absent such that the string remains straight as in the $\nu = 1$ case of Fig. 1.

3.4 Comparison to Asymptotically AdS backgrounds

The remarkably simple picture of confinement obtained here is consistent with the one derived in [9]. Ref. [9] considers a class of 5D dilatonic spacetimes which is asymptotically AdS in the UV and analogous to the \mathcal{M}_ν background in the IR. In our coordinates the AdS region is at large r , hence the IR region is similar to the \mathcal{M}_ν^- background considered here. Roughly speaking, spacetime continues into asymptotic AdS instead of stopping at the brane. The behavior of the string in the asymptotically AdS backgrounds can be easily understood using Prop. (3.12).

Let us consider a string anchored to the AdS boundary (or on a brane in the AdS region, i.e. at large r) with endpoints separation Δx in Minkowski distance. For small Δx , the string only knows about the AdS background and thus bends towards smaller r , as dictated by Prop. (3.12) with $\nu = 0$. Increasing Δx , the tip of the string enters in the non-AdS IR region. In this regime, if $\nu < 1$, the string keeps entering further into the IR since it still tends to bend towards smaller r . But if, instead, $\nu > 1$, the part of the string in the IR wants to bend towards large r as dictated by (3.12). That is, for $\nu > 1$ the tendencies in the UV and IR regions are opposite. As a result the string does not go beyond a certain point in the IR. These behaviors are sketched in Fig. 2.

This phenomenon of saturation matches the behavior reported in [9], which was identified in terms of a non-monotonicity in the scale factor. It turns out that this saturation implies confinement asymptotically. The confining behavior is easily understood from the viewpoint of our analysis, for example by replacing the shaded region in Fig. 1 by asymptotic AdS. At large Δx , for $\nu \geq 1$ the main contribution to the string length would be the straight segment, that implies confinement as shown in section 3.3.

4 Spacelike Geodesics

We first compute the geodesic equation from a general Einstein frame metric ansatz of the form

$$ds^2 = g_{xx}(r)\eta_{\mu\nu}dx^\mu dx^\nu + g_{rr}(r)dr^2. \quad (4.1)$$

Translation symmetry along Minkowski slices implies the existence of Killing vectors $K = \partial_\mu$. The Killing equation then implies

$$\frac{dx^\mu}{ds} = \frac{U^\mu}{g_{xx}(r)}, \quad (4.2)$$

with U^μ a velocity vector that characterizes the geodesic. We introduce $U^2 = \eta_{\mu\nu}U^\mu U^\nu$.

We focus on *spacelike* geodesics for which $U^2 > 0$. We find the geodesic equations

$$\frac{ds}{dr} = \frac{a(r)b(r)}{\sqrt{a(r) - U^2}}, \quad \frac{dx^\mu}{dr} = \frac{U^\mu}{a(r)} \frac{ds}{dr}, \quad (4.3)$$

with $a(r) = g_{xx}(r)$, $b(r) = \sqrt{\frac{g_{rr}(r)}{g_{xx}(r)}}$. Since $\frac{dr}{dx^\mu}$ vanishes if $a(r) = U^2$, the U constant is identified as $U \equiv \sqrt{a(r_0)}$ where r_0 is the coordinate of the ‘‘tip’’ of the geodesic.

4.1 Geodesics of \mathcal{M}_ν^- with no Black Hole

4.1.1 Solutions

Applying (4.3) to the \mathcal{M}_ν background with metric given by (2.4), we have $U^2 = r_0^2/L^2$. The general solutions to the geodesic equations take the form

$$s = -\frac{ir^{\nu^2+1}}{r_b^{\nu^2}\eta(\nu^2+1)r_0} {}_2F_1\left(\frac{1}{2}, \frac{1}{2}(\nu^2+1); \frac{1}{2}(\nu^2+3); \frac{r^2}{r_0^2}\right) + \text{cst}, \quad (4.4)$$

$$x^\mu = \frac{iL^2U^\mu r^{\nu^2-1}}{r_b^{\nu^2}\eta(1-\nu^2)r_0} {}_2F_1\left(\frac{1}{2}, \frac{1}{2}(\nu^2-1); \frac{1}{2}(\nu^2+1); \frac{r^2}{r_0^2}\right) + \text{cst}, \quad (4.5)$$

with $\nu \neq 1$ and $r_0 \neq 0$. The $\nu = 1$ case is treated in details in section 4.3.

If $r_0 = 0$, then $U^\mu = 0$ and $\Delta x^\mu = 0$. In this case,

$$s(r) = \begin{cases} \frac{\log(r)}{\eta} + \text{cst}, & \nu = 0 \\ \frac{r^{\nu^2}}{\eta r_b^{\nu^2} \nu^2} + \text{cst}, & \nu \neq 0 \end{cases}. \quad (4.6)$$

4.1.2 Shape

We focus on brane-to-brane spacelike geodesics in the \mathcal{M}_ν^- spacetime. These geodesics start and end on the brane at $r = r_b$, and extend in the bulk down to $r = r_0$. The separation of the endpoints on the brane is denoted by $\Delta x \equiv \sqrt{\eta_{\mu\nu}\Delta x^\mu \Delta x^\nu}$. The behavior of the geodesics differ among the $\nu < 1$, $\nu = 1$ and $\nu > 1$ cases. The behavior of the geodesics is depicted schematically in Fig. 3.

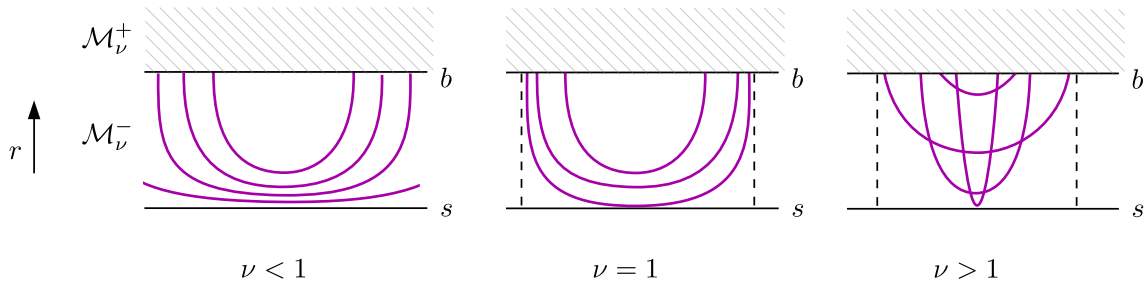


Figure 3. The brane-to-brane spacelike geodesics of the \mathcal{M}_ν^- spacetime. When evolving the tip of the geodesics r_0 from r_b to 0, the size of the base of the geodesic (Δx) increases indefinitely if $\nu < 1$, reaches a saturation if $\nu = 1$, and grows then shrinks back to 0 if $\nu > 1$. Lines b and s correspond to the brane and the singularity, respectively.

For $\nu < 1$, the base of the geodesics increases indefinitely when r_0 approaches 0, i.e. we have $\Delta x \in [0, \infty)$. In contrast, when $\nu = 1$ the base reaches a saturation i.e. the endpoint separation Δx is bounded from above. We obtain the domain $\Delta x \in [0, \frac{\pi L}{\eta r_b}]$ from the exact $\nu = 1$ formulas given in section 4.3. Finally, for $\nu > 1$, starting from $r_0 \sim r_b$, the base of the geodesics increases, reaches a maximum and then decreases to zero when r_0 approaches 0. Thus for $\nu > 1$ there exists *two* geodesics with same Δx .

Finally we mention that for $\nu \leq 1$, the geodesic in the $r_0 \rightarrow 0$ limit tends to take a square shape with a nearly flat part that approaches the $r = 0$ line.

4.1.3 Length

Using the expression (4.4), the length of the brane-to-brane geodesics is given by $\Delta s = 2|s(r_b) - s(r_0)|$. We find that Δs increases with Δx in all cases. The dependence of Δs as a function of Δx is shown in Fig. 4.

For a geodesic that stays near the brane, we have $r_0 \sim r_b$. In that case a simple linear relation appears,

$$\Delta s \approx \frac{r_b}{L} \Delta x \quad (r_0 \sim r_b \text{ or } \eta \Delta x \ll 1). \quad (4.7)$$

This formula applies both for $\nu \leq 1$ and for the short geodesics of $\nu > 1$.

We then study the limit of r_0 approaching $r = 0$. For $\nu = 0$ (AdS), Δs grows indefinitely when $r \rightarrow 0$. In contrast, for $\nu \neq 0$, Δs reaches a finite value $\Delta s|_{r \rightarrow 0} = \frac{2}{\eta \nu^2}$. These behaviors can be derived from Eq. (4.6).

The variation of Δs as a function of Δx is, at first order,

$$\Delta s \simeq \frac{2}{\eta \nu^2} + \frac{\sqrt{\pi} \Gamma\left(-\frac{\nu^2}{2}\right)}{\eta \Gamma\left(\frac{1}{2}(1 - \nu^2)\right)} \left[\frac{\eta \Gamma\left(\frac{1}{2}(3 - \nu^2)\right)}{\sqrt{\pi} \Gamma\left(1 - \frac{\nu^2}{2}\right)} \frac{r_b}{L} \Delta x \right]^{\frac{\nu^2}{\nu^2 - 1}} \quad (r_0 \ll r_b \text{ or } \eta \Delta x \gg 1), \quad (4.8)$$

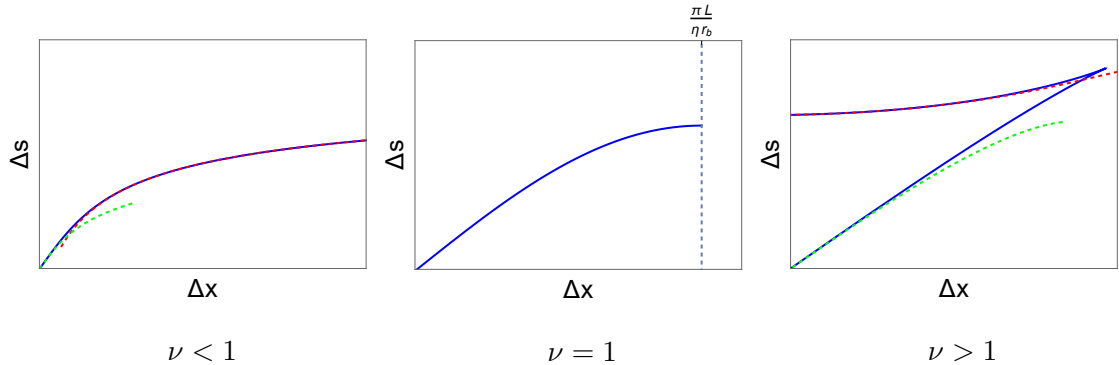


Figure 4. Length of the brane-to-brane spacelike geodesics Δs as a function of Δx . Plain lines are exact results for $\nu = 0.5, 1$ and 1.5 . Red and green dotted lines are respectively approximations for $r_0 \ll r_b$ (B.6) and (B.7), and for $r_0 \approx r_b$ (B.8) and (B.9).

for $\nu^2 < 2$ and

$$\Delta s \simeq \frac{2}{\eta\nu^2} + \frac{\eta r_b^2(\nu^2 - 2)}{4L^2}(\Delta x)^2 \quad (r_0 \ll r_b \text{ or } \eta\Delta x \gg 1), \quad (4.9)$$

for $\nu^2 > 2$. In the $\nu > 1$ case, these expressions describe the length of the long geodesics. The approximations of the geodesic lengths for $r_0 \sim r_b$ and $r_0 \ll r_b$ are shown in Fig. 4.

More detailed approximations are given in App. B.

4.2 Geodesics of \mathcal{M}_ν^- with a Black Hole

The \mathcal{M}_ν background admits a planar black hole solution given by the metric (2.7). Following the same steps as in section 4.1, the solutions for $s(r)$ and $x^\mu(r)$ in the presence of the black hole are

$$s(r) = \frac{1}{r_b^{\nu^2}\eta} \int dr \frac{r^{\nu^2-1}}{\sqrt{\left(1 - \left(\frac{r_h}{r}\right)^{4-\nu^2}\right) \left(1 - \frac{r_0^2}{r^2}\right)}}, \quad (4.10)$$

$$x^\mu(r) = \frac{L^2 U^\mu}{r_b^{\nu^2}\eta} \int dr \frac{r^{\nu^2-3}}{\sqrt{\left(1 - \left(\frac{r_h}{r}\right)^{4-\nu^2}\right) \left(1 - \frac{r_0^2}{r^2}\right)}}. \quad (4.11)$$

These integrals cannot be solved exactly for arbitrary ν . Here we focus on brane-to-brane geodesics with $r_h \gg r_0$.

We first compute the length of the geodesics going between brane and horizon, $\Delta s_h = |s(r_b) - s(r_h)|$. In the $r_h \gg r_0$ limit, the bending of the geodesics between r_b and r_h is negligible. The integral (4.10) can be performed exactly as (B.15). The geodesic distance

is approximately given by

$$\Delta s_h \simeq \begin{cases} \frac{1}{\eta} \operatorname{arccosh} \left(\frac{r_b^2}{r_h^2} \right), & \nu = 0 \\ \frac{2}{\eta \nu^2} - \frac{2\sqrt{\pi} \left(\frac{r_h}{r_b} \right)^{\nu^2} \Gamma \left(\frac{2(\nu^2-2)}{\nu^2-4} \right)}{\eta \nu^2 \Gamma \left(\frac{4-3\nu^2}{8-2\nu^2} \right)} & \nu > 0 \end{cases}, \quad (4.12)$$

where for $\nu > 0$ we have assumed $r_b \gg r_h$. For $\nu > 0$, the first term corresponds to the result from the brane to the singularity with no black hole, that can be read from (4.8). The second term is the correction due to the black hole. It is large for ν close to zero, and rapidly decreases for larger ν . The special cases $\nu = \sqrt{2}, 2, \dots$, need separate treatment but conclusions are analogous.

We turn to brane-to-brane geodesics. For $r_h > r_0$, the brane-to-brane geodesic reach $r = r_h$, then return to the brane. For $r_h \gg r_0$, the geodesics tend to have a square shape that “hugs” the horizon, see e.g. [88] for similar considerations. In this limit, the length of the brane-to-brane geodesic is approximately given by the sum of $2\Delta s_h$ and of the displacement along the horizon $\frac{r_h}{L} \Delta x$,

$$\Delta s \approx 2\Delta s_h + \frac{r_h}{L} \Delta x \quad (r_0 \ll r_h). \quad (4.13)$$

4.3 Geodesics in Linear Dilaton Spacetime

The solutions to the geodesic equation in the linear dilaton case ($\nu = 1$) take the simple form

$$s(r) = \frac{1}{\eta r_b} \sqrt{r^2 - r_0^2} + \text{cst}, \quad (4.14)$$

$$x^\mu(r) = \frac{U^\mu L^2}{\eta r_b r_0} \arctan \left(\sqrt{\frac{r^2}{r_0^2} - 1} \right) + \text{cst}. \quad (4.15)$$

In this spacetime, we find, like in AdS (B.4) and flat spaces, an explicit formula of the distance Δs between two arbitrary points (x_1^μ, r_1) , (x_2^μ, r_2) , as a function of the distance along Minkowski slices $\Delta x = \sqrt{\eta_{\mu\nu} (x_1 - x_2)^\mu (x_1 - x_2)^\nu}$. A direct calculation gives the distance

$$\Delta s = \frac{1}{\eta r_b} \sqrt{r_1^2 + r_2^2 - 2r_1 r_2 \cos \left(\frac{\eta r_b}{L} \Delta x \right)}. \quad (4.16)$$

This distance formula has remarkable properties that will be further used in a future work. Here we notice that, as can already be seen from (4.15), Δx features an upper bound. Using (4.16) we find for example that the brane-to-brane geodesic ($r_1 = r_2 = r_b$) has length

$$\Delta s = \frac{2}{\eta} \sin \left(\frac{\eta r_b}{2L} \Delta x \right). \quad (4.17)$$

We then see that the largest allowed Δx , corresponding to the argument being equal to $\pi/2$, is $\Delta x = \frac{\pi L}{\eta r_b}$. This is the upper bound on Δx reported in section 4.1.3. As a sanity check, at small Δx we recover $\Delta s \approx \frac{r_b}{L} \Delta x$.

5 Holographic Entanglement Entropy

In a given quantum system, the entanglement of a given subsystem with the rest of the system can be quantified using the entropy. This entanglement (or von-Neumann) entropy (EE) is defined via tracing out the states outside the subsystem. It can be viewed as the amount of entropy for an observer that only receives information from the subsystem. Entanglement entropy is typically used as a tool to understand quantum systems.

Entanglement entropy in holographic theories admits a simple geometric description [89–98]. The interplay of holographic entanglement entropy (HEE) with confinement has been explored in [64–75]. Here our goal is to understand HEE in the simple setup of dilaton gravity. We explore the HEE described by the \mathcal{M}_ν^- background, and also establish some properties of HEE for more general warped metrics.

The subsystem of our interest is supported on a region A of the brane. Focusing on a spacelike region, the HEE is given by the Ryu-Takayanagi formula [89]

$$S_A = \frac{\text{Area}(\gamma_A)}{4G_N}, \quad (5.1)$$

where γ_A is the surface of minimal area anchored to the boundary of A . We choose the simplest region for A : a $(d-1)$ -dimensional strip with width L_A .

In the following we first establish some properties for the general warped metric defined in (4.1), before turning to the detailed analysis of the \mathcal{M}_ν^- background.

5.1 Elementary Properties

We can identify two possible surfaces: *i*) a smooth surface generated by the shift of a curve with base $\Delta x = L_A$, and *ii*) a squared-shape surface that extends from the brane ($r = r_b$) down to $r = 0$. The surfaces are respectively denoted γ_\cup and γ_\sqcup and are depicted in Fig. 5.

We are interested in the behavior of S_A as a function of the strip width L_A . Anticipating the HEE results, the existence of these two surfaces is the cause of *phase transitions* in the EE, which happen because either γ_\cup or γ_\sqcup have minimal area depending on the subsystem size.

The surfaces in Fig. 5 are parametrized by an embedding $x^M = F(\sigma^m)$ where σ^m are the d coordinates for the points belonging to the surface. We choose $F(\sigma^m) = (\sigma^m, u(\sigma^1))$, such that the σ^m are identified with $(r, x^0, x^1, \dots, x^{d-2})$. In Fig. 5, x^{d-1} is the direction which crosses the strip. The profile of the minimal surface is given by $x^{d-1} = u(r)$. The vertical sides of the square surface correspond to $x^{d-1} = \text{cst}$. The longitudinal directions collectively represent the other (x^0, \dots, x^{d-2}) directions. The induced metric for the surface is then

$$ds_{\text{ind}}^2 = \left(g_{rr}(r) + u'^2(r) g_{xx}(r) \right) dr^2 + g_{xx}(r) \left(-(dx^0)^2 + (dx^1)^2 + \dots + (dx^{d-2})^2 \right). \quad (5.2)$$

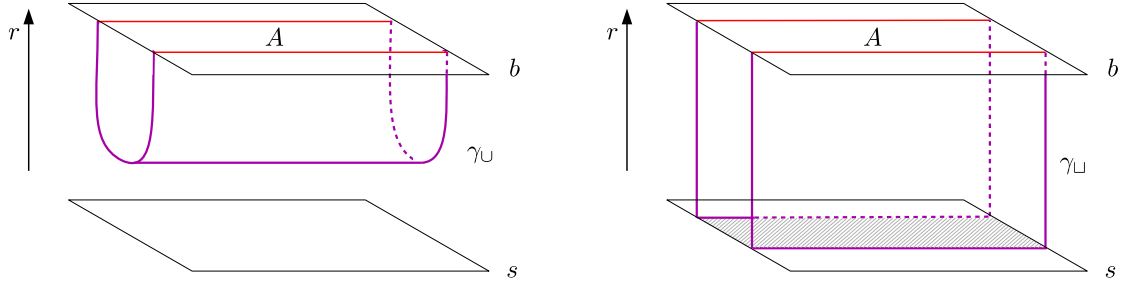


Figure 5. The candidate minimal surfaces anchored to the surface of a static $(d-1)$ -strip on the brane. Left: The smooth surface. Right: The square surface.

5.1.1 Smooth Surface

From the induced metric (5.2), we can compute the spatial area of the smooth surface as

$$\text{Area}(\gamma_U) = 2A_{d-2} \int_{r_0}^{r_b} dr a(r)^{\frac{d-1}{2}} \sqrt{b^2(r) + u'^2(r)}, \quad (5.3)$$

where $A_{d-2} = \int dx^1 \cdots dx^{d-2}$. We remind the definitions $a(r) = g_{xx}(r)$, $b(r) = \sqrt{\frac{g_{rr}(r)}{g_{xx}(r)}}$.

The surface is minimal when the $u(r)$ function satisfies the Euler-Lagrange equation

$$\frac{du(r)}{dr} = U \frac{b(r)}{\sqrt{a(r)^{d-1} - U^2}}. \quad (5.4)$$

Here U is a constant that characterizes the curve $x^{d-1} = u(r)$. Since $\frac{dr}{du} = 0$ determines the tip of the curve at $r = r_0$, we have $U = a(r_0)^{\frac{d-1}{2}}$. The strip width L_A and the tip of the curve r_0 are tied due to the solutions of (5.4), i.e. we have $L_A = L_A(r_0)$. For $d = 2$ the minimal surface reduces to the geodesic studied in section 4.

5.1.2 Square Surface and Singularity

The area of the square surface is the one of the vertical piece plus the one of the strip at $r = 0$. In that case L_A is a free parameter.

The existence of γ_U requires that straight geodesics exist in a first place. In terms of the general warped metric (4.1), this is true if there is a value of r_0 such that the metric coefficient $a(r)$ satisfies $a(r_0) \equiv 0$. The bottom part of the square surface is localized at r_0 , which implies that its area is vanishing due to the vanishing of the scale factor. Hence we have always that

$$\text{Area}(\gamma_U) = 2A_{d-2} \int_0^{r_b} dr a(r)^{\frac{d-1}{2}} b(r), \quad (5.5)$$

for any strip width L_A .

Assuming conformal coordinates (x^μ, z) in the general metric such that $b(z) = 1$ for all z , the existence of γ_U requires $a(z_0) \equiv 0$, which implies that z_0 is a metric zero. Applying

Prop. (2.11), this implies that there is a curvature singularity at $z = 0$ on which the square surface ends.

5.1.3 A Necessary Condition for HEE phase transition

The area for the square surface may be finite or infinite, depending on the behavior of the integral $\int_0^{r_b} dr a(r)^{\frac{d-1}{2}} b(r)$. If the integral diverges, the γ_{\sqcup} has infinite area and thus the minimal area is the one of γ_{\cup} . In that case, no phase transition can happen in the HEE. Therefore,

A HEE phase transition can occur only if the integral $\int_0^{r_b} dr a(r)^{\frac{d-1}{2}} b(r)$ is finite.

(5.6)

This is a necessary condition. This condition is automatically satisfied if there is a metric zero at finite conformal distance. Thus the possibility of a HEE phase transition is related via Prop. (2.11) to the existence of a singularity at finite conformal distance.

5.1.4 The Near-Brane Surface

When r_0 is close to r_b , the smooth surface stays near the brane. In that limit the equations (5.3) and (5.4) are dominated by the square root term $(a(r)^{d-1} - a(r_0)^{d-1})^{-1/2}$, while the other factors can be taken at $r \sim r_b$. This implies that

$$\text{Area}(\gamma_{\cup}) \stackrel{r_0 \sim r_b}{\approx} A_{d-2} L_A a(r_b)^{\frac{d-1}{2}}. \quad (5.7)$$

That is, the area of γ_{\cup} tends to the area of the basis region, $\text{Area}(\gamma_{\cup}) \approx \text{Area}(A)$. The (5.7) limit can also be understood as the area for “small” γ_{\cup} , since the approximation is valid in the small L_A limit.

5.2 Phase Transition and Boundaries

This section establishes some properties of the HEE for the general warped metric of (4.1). All the properties obtained here appear explicitly in the case of the \mathcal{M}_{ν}^{-} background presented in section 5.3, see in particular Fig. 6.

A necessary condition for a phase transition of HEE to occur is that the width of the base of the γ_{\sqcup} surface be bounded from above, i.e. $L_A < L_A^{\max}$ with $L_A^{\max} < \infty$. In such a situation, whenever one considers a strip A with $L_A > L_A^{\max}$, only the γ_{\cup} remains available, hence γ_{\sqcup} is automatically the minimal surface. Here we establish a relation between the boundedness of the base of γ_{\cup} , i.e. the existence of a finite L_A^{\max} , and the existence of a singularity at finite conformal distance.

As seen in section 2.3, the spacetime background may feature either a regular or a conformal timelike boundary along constant r slices. Since this distinction is done using conformal coordinates, here we go to conformal coordinates (x^{μ}, z) , that imply $b(z) = 1$ for any z such that the warped metric (4.1) is manifestly conformally flat. We assume in this subsection that the metric coefficients are *strictly monotonic*.

Using the Euler-Lagrange equation (5.4), we know that the width of the base of γ_U satisfies

$$L_A(z_0) = U \int_{z_0}^{z_b} \frac{dz}{\sqrt{c(z) - U^2}}, \quad (5.8)$$

where $c(z) = a(z)^{d-1}$ and $U^2 = c(z_0)$, with z_0 the coordinate of the tip of the curve. If $c(z)$ is monotonically increasing (resp. decreasing) we have $z_0 < z_b$, (resp. $z_0 > z_b$), such that $c(z) > c(z_0)$ under the integral in all cases. In the following we choose c to be increasing and thus $z_0 < z_b$.

We denote the domain of $a(z)$ by $[z_*, z_b]$. The lower bound z_* may be either finite or infinite. We assume in this subsection that U can reach 0, which is required for the square surface to exist (see section 5.1.2). Since $U^2 = c(z)$ with c monotonic, this condition corresponds necessarily to having $c(z_*) = 0$. Using Prop. (2.11), if z_* is finite then there is a curvature singularity at $z_* \equiv z_s$. If z_* is infinite, no statement can be made and z_* can be simply thought of as the boundary for z .

5.2.1 Sufficient Conditions for HEE Phase Transition

We rewrite the integral in (5.8) as

$$\int_{U^2}^{y_b} \frac{dy}{c'[c^{-1}(y)]\sqrt{y - U^2}}, \quad (5.9)$$

where we used the change of variable $c(z) \equiv y$, with $y_b \equiv c(z_b)$, $y_0 \equiv c(z_0) = U^2$. The function c^{-1} is the inverse of the c function and $c'[x]$ is the derivative of c with respect to its argument x .

Since by assumption the c function is monotonic on the open interval (z_*, z_b) , there exists $B > 0$ such that $c'(z) > B$ for all $z \in (z_*, z_b)$. Hence the inverse $1/c'(z)$ is defined on (z_*, z_b) . However it is not guaranteed that $1/c'(z)$ is defined at the endpoints, where it might blow up, e.g. $1/c'(z_*) = \infty$. In such a case the integral (5.9) is improper.

A sufficient condition for the integral (5.9) to be finite is if the lower bound z_* is finite and $1/c'(z)$ is defined on the *closed* interval $[z_*, z_b]$. In that case, having a continuous function on a closed interval, the boundedness theorem implies that there exists an upper bound \bar{B} on $1/|c'(z)|$ on $[z_*, z_b]$. As a result the integral (5.9) is bounded from above by $\bar{B} \int_{U^2}^{y_b} dy (y - U^2)^{-1/2} = 2\bar{B} \sqrt{y_b - U^2}$. The comparison theorem for integrals then implies that (5.9) is bounded from above for any U . Going back to the definition (5.8) we use that U is bounded from above since $c(z_0) < c(z_b)$ for all $z_0 < z_b$ because c is monotonic increasing. It follows that $L_A(z_0)$ is bounded from above for any z_0 , i.e. there exists $L_A^{\max} < \infty$. The same conclusion happens if one chooses the convention that c is decreasing and $z_0 > z_b$. Putting the pieces together, we conclude that

If the function $1/c'(z)$ is defined on the *closed* interval $[z_*, z_b]$ with finite z_* , then the holographic entanglement entropy exhibits a phase transition. (5.10)

Since having a metric zero at finite z_* implies a curvature singularity by Prop. (2.11), the condition in (5.10) requires $1/c'(z)$ to be defined on the singularity $z_* \equiv z_s$.

We emphasize that (5.10) is only a sufficient condition for the existence of HEE phase transition. For example, when applied to the \mathcal{M}_ν^- metric, for which $c(z) \propto z^{\frac{2(d-1)}{\nu^2-1}}$ and a regular boundary $z_s = 0$ exists for $\nu > 1$, we have $1/c'(z) \propto z^{\frac{2d-1-\nu^2}{1-\nu^2}}$. This is finite at $z \rightarrow z_s$ only for $\nu > \sqrt{2d-1}$, which ensures the existence of the HEE phase transition in this range of ν — but not for lower ν . Since the absence of bad singularity requires $\nu < 2$ in any dimension (see section 2.3), a bound follows from condition (5.10) only for $d = 2$.

We find a slightly better sufficient condition by bounding $dc^{-1}(y)/dy \equiv [c^{-1}]'(y) = 1/c'[c^{-1}(y)]$ with the U -dependent upper bound $[c^{-1}]'(U^2)$. Such a bound is set up to include the situation where $[c^{-1}]'(y)$ blows up at $y \rightarrow 0$, that is not taken into account by the sufficient condition (5.10). We put this upper bound in the definition (5.8) and require finiteness for any U . We obtain that L_A is bounded from above for any U (i.e. any z_0) if the condition

$$U \times [c^{-1}]'(U^2) < \infty \quad (5.11)$$

is satisfied for all U . Using $U^2 = c(z_0)$ and $c(z) = a(z)^{d-1}$, we obtain the final condition that is summarized as

If the function $\frac{a^{\frac{3-d}{2}}(z_0)}{a'(z_0)}$ is bounded from above for all $z_0 \in (z_*, z_b]$, then the holographic entanglement entropy exhibits a phase transition.

(5.12)

When applied to the \mathcal{M}_ν^- metric, this gives the sufficient condition $\nu > \sqrt{d}$.

5.2.2 Pairs of Smooth Surfaces

In the presence of the singularity at finite conformal distance, the fact that $L_A(z_0)$ tends to zero when $z_0 \rightarrow z_s$ implies that there exist *two* smooth surfaces γ_U , that both solve the Euler-Lagrange equation, for a given $L_A < L_A^{\max}$. This is because, for a given L_A , in addition to the large surface with $z_0 \sim z_s$, there is always a small surface closer to the brane, whose area is given by (5.7). By continuity of L_A in z_0 , for any $L_A < L_A^{\max}$ there must exist two smooth surfaces with different z_0 .

In summary, the presence of a singularity at finite conformal distance implies the existence of a pair of smooth surfaces.

5.3 Holographic Entanglement Entropy in the \mathcal{M}_ν^- background

For $d = 2$ the solutions of (5.4) are the geodesics presented in section 4, see Fig. 4. Based on the properties established in the previous subsections, we can already deduce that the HEE behavior for $d > 2$ is analogous to the $d = 2$ case. But in the \mathcal{M}_ν^- background we can actually compute the minimal surfaces directly. This is because the Euler-Lagrange equation (5.4) is proportional to a geodesic equation (4.3) in the $\mathcal{M}_{\nu'}^-$ spacetime, where

$$\nu'^2 = \frac{\nu^2 + d - 2}{d - 1} \quad (5.13)$$

for $\nu \neq 1$. Moreover, in the linear dilaton case, a direct calculation shows that $\nu' = \nu = 1$.

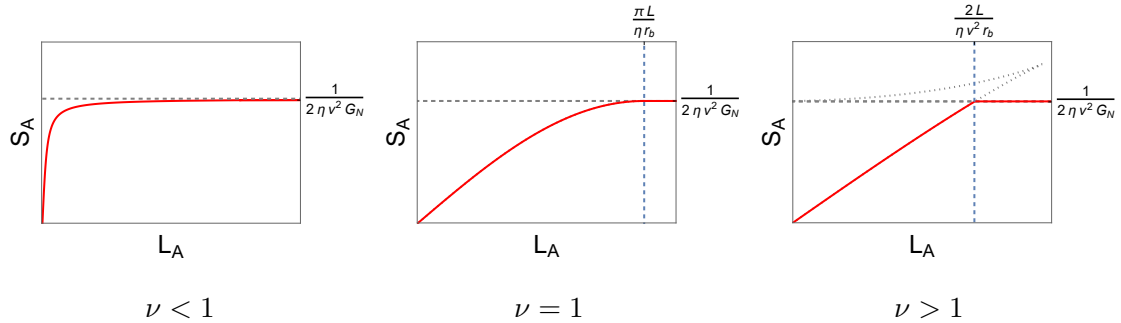


Figure 6. Holographic entanglement entropy from the \mathcal{M}_ν^- background with $d = 2$ spatial dimensions, shown as a function of the strip width. A second order phase transition occurs if $\nu = 1$, while a first order phase transition occurs if $\nu > 1$.

It follows that the behavior of the minimal surfaces for $d > 2$ is qualitatively analogous to the one of the $d = 2$ geodesics. In particular, the linear dilaton has always the status of critical case between two qualitatively different regimes. The numerical results for the HEE in \mathcal{M}_ν^- with $d = 2$ are presented in Fig. 6.

For $\nu < 1$, we obtain that S_A reaches a plateau at large L_A , with value $S_A^{\max} = \frac{A_{d-2}}{2G_N\eta(\nu^2+d-2)} \left(\frac{r_b}{L}\right)^{d-2}$. The existence of HEE plateaux has been noted in the literature, typically at finite temperature, see [94]. This saturation corresponds to the saturation of the Araki-Lieb inequality [99]. Here we observe this saturation phenomenon at *zero temperature*. For $d = 2$ the plateau occurs for $\nu > 0$, and may be viewed as a consequence of the singularity. Notice however that for $d > 2$ the plateau occurs for any $\nu \geq 0$, hence we do not draw further conclusion. From the viewpoint of the general metric (4.1), a HEE plateau occurs when the integral $\int_0^{r_b} dr a(r)^{\frac{d-1}{2}} b(r)$ is finite.

For $\nu = 1$, we know that the base of the smooth surface is bounded from above. This follows from the direct calculations of linear dilaton geodesics in section 4 and from application of the condition (5.12) from the viewpoint of the general warped metric. The upper bound is $\frac{\pi L}{\eta r_b(d-1)}$. There is thus necessarily a phase transition, which happens to occur precisely at this value. Using the explicit formula for the linear dilaton geodesic length (4.16), we find that $S_A^{\nu=1}$ experiences a discontinuity in its second derivative. Therefore there is a *second order* phase transition in the HEE.

For $\nu > 1$ we observe that the base of the geodesics is bounded and that a doubling of the geodesics occurs. From the viewpoint of the general metric, we understand that this phenomenon is a consequence of the curvature singularity that truncates space, see section 5.2. The phase transition occurs when the area of the smaller smooth surface crosses the area of the square surface. We find that this occurs approximately at $L_A \simeq \frac{2L}{\eta(\nu^2+d-2)r_b}$. The first derivative is discontinuous, hence the HEE experiences a *first order* phase transition. The behavior of the areas and of the transition resembles the ones obtained in stringy setups in [64, 71, 73, 75]. In short, the curvature singularity at finite conformal distance implies a HEE first order phase transition.

6 Stability and the Radion Effective Action

In this section and the next, we study the brane-dilaton system globally. To this end, we put the classical bulk solutions (see [81]) into the fundamental action \mathcal{S} , defined in (2.1). This defines a “holographic” on-shell action that depends only on the brane location r_b and the value of the dilaton on the brane, ϕ_b , $\mathcal{S}_{\text{on-shell}}[r_b, \phi_b]$. We restrict the spacetime dimension to $D = 5$ for simplicity.

6.1 The Effective Potential

At zero-th order in the fluctuations, $\mathcal{S}_{\text{on-shell}}$ corresponds to an effective potential $\mathcal{S}_{\text{on-shell}} \equiv -\int d^4x V_{\text{eff}}(r_b, \phi_b)$. In [81] it was found

$$V_{\text{eff}} = U_b(\phi_b) \left(\frac{r_b}{L}\right)^4, \quad U_b(\phi_b) = V_b(\phi_b) + \Lambda_b \mp 6M_5^3 \eta(\phi_b), \quad (6.1)$$

for \mathcal{M}_ν^\mp . We introduced the dilaton-dependent scale $\eta(\phi_b) = k e^{\nu \bar{\phi}_b}$, with $\eta(v_b) \equiv \eta$ at the minimum $\phi_b \equiv v_b$.

Stability along the r_b direction requires to tune the 4D cosmological constant to $\Lambda_b = \pm 6M_5^3 \eta$ for \mathcal{M}_ν^\mp . Stability along the ϕ_b direction requires $U_b'' > 0$, which translates as a condition on V_b [81]. In the \mathcal{M}_ν^- spacetime such a vacuum is only metastable since V_{eff} is unbounded from below at large ϕ_b . We will see in section 7.2 that this feature is exacerbated in the presence of a very large black hole.

6.2 The Radion

Both the dilaton and spacetime can fluctuate around the configuration determined by (r_b, v_b) . Such fluctuations contribute to quantum corrections to geometric entropy formulas such as the one of HEE [95, 97, 98] as well as black hole entropy (see e.g. [100]).

Upon gauge fixing, these scalar fluctuations reduce to a single degree of freedom, usually called the *radion* field (see [81, 101]). It was shown in [81] that the radion spectrum in \mathcal{M}_ν^\pm always contains an isolated mode $R_0(x)$, that we refer to as *the* radion mode. The rest of the radion spectrum may be either discrete or continuous depending on ν , see summary table 1. Notice that this is tied to the singularity being either at finite or infinite conformal distance.

6.2.1 Definition

We consider the fluctuation of the dilaton and of the scalar sector of the fluctuations of the metric. In conformal coordinates, upon gauge-fixing (see [81, 101]) the following parametrization can be used:

$$ds^2 = e^{-2A(z)} \left[e^{-2F(x,z)} \eta_{\mu\nu} dx^\mu dx^\nu + (1 + 2F(x,z))^2 dz^2 \right],$$

$$\bar{\Phi}(x, z) = \bar{\phi}(z) + \bar{\varphi}(x, z). \quad (6.2)$$

It was shown in [81] that the equations of motion relate the dilaton fluctuation $\varphi(x, z)$ to the $F(x, z)$ fluctuation by

$$\bar{\phi}'(z)\bar{\varphi}(x, z) = (\partial_z - 2A'(z)) F(x, z). \quad (6.3)$$

We introduce $F(x, z) = F_0(z)R_0(x) + \dots$ and $\varphi(x, z) = \varphi_0(z)R_0(x) + \dots$, where $F_0(x)$ is the profile of the radion mode and the ellipses encode the distribution of the other modes, that may be either discrete or continuous [81].

6.2.2 Radion profile

The equation of motion for the F fluctuation is [32, 81, 101]

$$\partial_z^2 F(x, z) + \frac{1 + 2\nu^2}{\nu^2 - 1} \frac{1}{z} \partial_z F(x, z) - p^2 F(x, z) = 0. \quad (6.4)$$

The field F satisfies the following boundary conditions:

- i) Regularity at $z = 0$ if $z \in (0, z_b]$, or at $z \rightarrow \infty$ if $z \in [z_b, \infty)$.
- ii) Boundary condition at the brane [81]:

$$B_{\pm}(p^2) \equiv \left(\partial_z - 2A'(z) \pm \frac{2p^2 e^A}{U_b''} \right) F(x, z) \Big|_{z=z_b} = 0, \quad (6.5)$$

where the $+$ sign stands for $z \in (0, z_b]$, i.e. for $\mathcal{M}_{\nu < 1}^+$ and $\mathcal{M}_{\nu > 1}^-$, and the $-$ sign stands for $[z_b, \infty)$, i.e. for $\mathcal{M}_{\nu < 1}^-$ and $\mathcal{M}_{\nu > 1}^+$.

Eq. (6.5) constitutes the eigenvalue equation. In any warped background, $B_{\pm}(p^2)$ is proportional to the inverse Green's function, e.g. $B_{\pm}(p^2) \propto 1/G_{\pm}(z_b, z_b; p^2)$, hence the zeros of $B_{\pm}(p^2)$ are the poles of the Green's function (see [32, 102]). Solving for a small mass $m_0 \ll \eta$ we find the profiles corresponding to the radion mode R_0 ,

$$F_0(z) \simeq \begin{cases} C_F \left(\frac{z}{z_b} \right)^{2\gamma} & \text{in } \mathcal{M}_{\nu}^+ \\ C_F \left(1 + \frac{m_0^2}{4(\gamma-1)} z^2 \right) & \text{in } \mathcal{M}_{\nu}^- \end{cases} \quad (6.6)$$

and

$$\varphi_0(z) \simeq \begin{cases} \sqrt{3M_5^3} C_F \nu \left(\frac{z}{z_b} \right)^{2\gamma} & \text{in } \mathcal{M}_{\nu}^+ \\ -2\sqrt{3M_5^3} \frac{C_F}{\nu} \left(1 - \frac{\nu^2 - 1}{6} m_0^2 z^2 \right) & \text{in } \mathcal{M}_{\nu}^- \end{cases}. \quad (6.7)$$

The normalization constant is determined by substituting the solutions in the on-shell action and requiring canonical normalization,

$$S_{R_0, \text{kin}} = - \int d^4x dz e^{-3A(z)} (6M_5^3 |F_0(z)|^2 + |\varphi_0(z)|^2) (\partial_{\mu} R_0)^2 \equiv - \frac{1}{2} \int d^4x (\partial_{\mu} R_0)^2, \quad (6.8)$$

which sets

$$C_F = \begin{cases} \frac{|1-\nu^2|}{\sqrt{2}} \frac{\eta^{3/2} z_b}{\sqrt{3M_5^3}} & \mathcal{M}_\nu^+ \\ \frac{\nu|1-\nu^2|}{2} \frac{\eta^{3/2} z_b}{\sqrt{3M_5^3}} & \mathcal{M}_\nu^- \end{cases} . \quad (6.9)$$

6.3 Radion Mass from the On-Shell Action

We show how to compute the radion mass directly from the on-shell action. This provides an important consistency check of the equation of motion and boundary condition (6.4), (6.5), from which the mass can be independently derived. This is also a necessary step to further derive the radion effective action, including its interactions with other quantum fields.

We first rewrite the full renormalized on-shell action as

$$\mathcal{S} = \mathcal{S}_{\text{bulk}}^{\text{ren}} + \mathcal{S}_{\text{brane}} + \mathcal{S}_{\text{GHY}} , \quad (6.10)$$

with

$$\mathcal{S}_{\text{bulk}}^{\text{ren}} = \int d^5x \sqrt{g} \left(\frac{M_5^3}{2} {}^{(5)}R - \frac{1}{2} (\partial_M \phi)^2 - V(\phi) \right) + \mathcal{S}_{\text{ct}} , \quad (6.11)$$

$$\mathcal{S}_{\text{brane}} = - \int_{\text{brane}} d^4x \sqrt{\bar{g}} (V_b(\phi) + \Lambda_b) , \quad (6.12)$$

$$\mathcal{S}_{\text{GHY}} = M_5^3 \int_{\text{brane}} d^4x \sqrt{\bar{g}} K . \quad (6.13)$$

The counterterm is given by [81, 103]

$$\mathcal{S}_{\text{ct}} = 2M_5^3 \int_{\Sigma} d^4x \sqrt{h} \eta(\phi_{\Sigma}) , \quad (6.14)$$

with Σ a cutoff surface located at $r_{\Sigma} \gg r_b$, and $h_{\mu\nu}$ the induced metric on Σ .

We expand the action at quadratic order in the radion field $R(x)$. Notably, the expansion of the metric determinant is

$$g \equiv |\det g_{MN}| = e^{-5A(z)} \left(1 - 2F(x, z) - \frac{5}{2} F(x, z)^2 + \dots \right) . \quad (6.15)$$

Focussing on the radion mode R_0 , we substitute the expressions of the F_0 , φ_0 profiles (6.6) and (6.7) in the renormalized on-shell action. We find the following contributions at

quadratic order:

$$\mathcal{S}_{\text{bulk,quad}}^{\text{ren}} = \begin{cases} \frac{16-24\nu^2-3\nu^4}{6(1-\nu^2)^2} \frac{1}{z_b^2} \int d^4x R_0(x)^2 & (\mathcal{M}_\nu^+) \\ -\frac{13}{3} \frac{\nu^2}{(1-\nu^2)^2} \frac{1}{z_b^2} \int d^4x R_0(x)^2 & (\mathcal{M}_\nu^-) \end{cases} \quad (6.16)$$

$$\mathcal{S}_{\text{brane,quad}} = \begin{cases} -\frac{U_b''\nu^2-2\eta(4-\nu^2)^2}{4(1-\nu^2)^2} \frac{1}{\eta z_b^2} \int d^4x R_0(x)^2 & (\mathcal{M}_\nu^+) \\ -\frac{U_b''+18\nu^2\eta}{2(1-\nu^2)^2} \frac{1}{\eta z_b^2} \int d^4x R_0(x)^2 & (\mathcal{M}_\nu^-) \end{cases} \quad (6.17)$$

$$\mathcal{S}_{\text{GHY,quad}} = \begin{cases} -\frac{8}{3} \frac{(4-3\nu^2)}{(1-\nu^2)^2} \frac{1}{z_b^2} \int d^4x R_0(x)^2 & (\mathcal{M}_\nu^+) \\ \frac{40}{3} \frac{\nu^2}{(1-\nu^2)^2} \frac{1}{z_b^2} \int d^4x R_0(x)^2 & (\mathcal{M}_\nu^-) \end{cases} \quad (6.18)$$

We have made use of the following identities

$$V_b(v_b) = 0, \quad V_b'(v_b) = \pm 2\sqrt{3M_5^3\nu\eta}, \quad V_b''(v_b) = U_b''(v_b) \pm 2\nu^2\eta, \quad \Lambda_b = \pm 6M_5^3\eta, \quad (6.19)$$

for \mathcal{M}_ν^\mp . The first condition is a choice with no loss of generality. The second and third conditions follow from the definition of the brane-localized effective potential $U_b(\phi_b)$ given in (6.1), using that U_b has a minimum at $\phi_b = v_b$. The fourth condition corresponds to the tuning that ensures $U_b(v_b) = 0$, so that the effective radion potential $V_{\text{eff}}(r_b, v_b) = U_b(v_b) \left(\frac{r_b}{L}\right)^4$ has a flat direction in r_b .

The full radion quadratic action is then

$$\mathcal{S}_{\text{quad}} = \begin{cases} -\frac{\nu^2}{4(1-\nu^2)^2} U_b'' \frac{1}{\eta z_b^2} \int d^4x R_0(x)^2 & (\mathcal{M}_\nu^+) \\ -\frac{1}{2(1-\nu^2)^2} U_b'' \frac{1}{\eta z_b^2} \int d^4x R_0(x)^2 & (\mathcal{M}_\nu^-) \end{cases}, \quad (6.20)$$

from which we identify the radion mass

$$m_0^2 = \begin{cases} \frac{\nu^2}{2(1-\nu^2)^2} U_b'' \frac{1}{\eta z_b^2} & (\mathcal{M}_\nu^+) \\ \frac{1}{(1-\nu^2)^2} U_b'' \frac{1}{\eta z_b^2} & (\mathcal{M}_\nu^-) \end{cases}. \quad (6.21)$$

This result agrees with the pole mass obtained from the radion propagators [81] in the limit of small U_b'' .

We have similarly checked the mass term at next-to-leading order in the U_b'' expansion, finding again consistency with the result from [81].

7 Holographic Thermal Phase Transitions

We turn to the on-shell action in the presence of the bulk black hole.

As discussed in Ref. [81], the black hole is always in the \mathcal{M}_ν^- region. We use the (x^μ, r) coordinates with $r \in (0, r_b]$. Throughout this section we use a \mathbb{Z}_2 orbifold convention as in [104] which implies that the spacetime is mirrored on the other side of the brane. The domain of integration of r is thus doubled in the action. A notable implication is that the entropy of the black hole horizon is doubled when using this convention, see e.g. Ref. [60].

The black hole metric is given in (2.7). We assume that the brane is outside the black hole, $r_h < r_b$. We define $f(r_b) \equiv f_b$, with $f(r) = 1 - \left(\frac{r_h}{r}\right)^{4-\nu^2}$. We introduce the brane proper time $dt = \frac{r_b}{L} \sqrt{f(r_b)} d\tau$, with τ the comoving time from the comoving volume element $d^4x = d\tau d^3x$.

We find the on-shell action

$$\mathcal{S}_{\text{on-shell}} = - \int dt d^3x \left(\frac{r_b}{L}\right)^3 U_b(\phi_b), \quad U_b(\phi_b) = U_b^0(\phi_b) + 6M_5^3 \eta(\phi_b) \Delta(r_b, r_h), \quad (7.1)$$

with

$$\Delta(r_b, r_h) = \frac{1}{\sqrt{f_b}} \left(\sqrt{f_b} - 1 + \frac{(2 + \nu^2)}{6} (1 - f_b) \right). \quad (7.2)$$

The $U_b^0(\phi_b)$ term in (7.1) is $U_b^0(\phi_b) = U_b(\phi_b)|_{r_h \rightarrow 0}$, i.e. it is the brane-localized effective potential with no black hole given in (6.1). The effect of the black hole is fully encoded into the second term.

7.1 Thermodynamics on the Brane

From the viewpoint of the brane, the black hole contributes as *perfect fluid*, see [27, 34, 35, 81]. It was shown in [81] that the thermodynamics of this holographic fluid essentially mirrors the bulk black hole thermodynamics.

Volume

A first thermodynamic variable defined on the brane is the volume (V_b), which is related to the comoving volume $V_3 = \int d^3x$ by

$$V_b \equiv V_3 a^3(r_b), \quad (7.3)$$

with the scale factor

$$a(r_b) \equiv e^{-A(r_b)} = \frac{r_b}{L}. \quad (7.4)$$

Temperature

The fluid temperature (T_b) is related to the Hawking temperature T_h as [81]

$$T_b = \frac{T_h}{a(r_b)} = \frac{4 - \nu^2}{4} \frac{\eta}{\pi} \left(\frac{r_b}{r_h}\right)^{\nu^2 - 1}. \quad (7.5)$$

The Hawking temperature T_h is obtained by requiring the absence of conical singularity near the horizon (see e.g. [35] for the general planar black hole case).

We can notice that T_b decreases (increases) with r_b/r_h for $\nu < 1$ ($\nu > 1$). For $\nu = 1$, the fluid has a constant temperature $T_b|_{\nu=1} = \frac{3\eta}{4\pi}$ whenever it exists.

Free energy

The on-shell action can be expressed in Euclidean time ($t = -it_E$) as $i\mathcal{S}_{\text{on-shell}} = -\mathcal{S}_{\text{on-shell}}^E$. When ϕ_b is at its vev v_b^T , we identify the free energy of the system:⁸

$$\mathcal{S}_{\text{on-shell}}^E \Big|_{\phi_b=v_b} \equiv \beta V_b F. \quad (7.6)$$

Here F is the free energy density and $\beta = \frac{1}{T}$ the inverse temperature of the system.

At equilibrium, we have $T = T_b$ as imposed by the absence of conical singularity upon Euclidean time compactification. In this section we will briefly discuss the out-of-equilibrium case of $T \neq T_b$, in which case the free energy has an extra contribution $F_{\text{cone}} \propto (T - T_b)$ [61, 105]. The T_b temperature can be identified even in case of non-vanishing conical singularity, see [105].

The free energy of the system is given by

$$F = U_b^0 + F_{\text{fluid}} + F_{\text{cone}}, \quad F_{\text{fluid}} = 6M_5^3 \eta \Delta(T_b), \quad (7.7)$$

with $\Delta(T_b) \equiv \Delta(r_b, r_h)$. In the small black hole limit $r_h \ll r_b$, the fluid free energy density simplifies to

$$F_{\text{fluid}} \Big|_{r_h \ll r_b} \approx -(1 - \nu^2) \eta M_5^3 \left(\frac{r_h}{r_b} \right)^{4-\nu^2}. \quad (7.8)$$

This reproduces the result presented in [81]. In this limit the free energy is negative for $\nu < 1$ and positive for $\nu > 1$. We will see in section 7.2 that this is not true away from the small r_h limit, which will be the cause of a phase transition. In contrast, (7.2) implies that the vanishing of F_{fluid} for $\nu = 1$ remains exact for any r_h .

A typical out-of-equilibrium situation is when a thermal bath with temperature T is localized on the brane, while the black hole/holographic fluid has $T_b \ll T$. The thermal bath radiates into the bulk, feeding the out-of-equilibrium black hole. In such a setup the bulk is non-empty, a Vaidya-type metric has to be used [106, 107]. Here we will discuss this case only qualitatively.

7.2 Phase Transitions

The information about phase transitions is encoded into the $\Delta(T_b)$ function. A phase with no fluid, i.e. with no black hole ($r_h \rightarrow 0$), has $f_b|_{r_h \rightarrow 0} = 1$ and thus $\Delta(T_b)|_{r_h \rightarrow 0} = 0$. The existence of phase transitions is thus controlled by the sign of $\Delta(T_b)$.

Critical temperature. The critical value of T_b at which a phase transition occurs is denoted by T_c and is determined by $\Delta(T_c) = 0$. Written in terms of f_b , the solutions are given by

$$\sqrt{f_{b\pm}} = \frac{3 \pm |\nu^2 - 1|}{2 + \nu^2}. \quad (7.9)$$

⁸Notice that in the presence of a black hole, the vev (v_b^T) is different from the vev with no black hole (v_b), and thus $U_b^0 \equiv U_b^0(v_b^T)$ is generically non-vanishing in the former case. Nevertheless, this effect is small for r_b large enough compared to r_h , as can be seen in Fig. 8.

We also know that physical solutions must satisfy $f_b \leq 1$.

Latent heat. The order of the phase transition is controlled by the associated latent heat per unit volume, ℓ_b . The transition is first order if $\ell_b \neq 0$ and second order if $\ell_b = 0$. The latent heat for a phase transition at temperature T_c is defined as $L_b = T_c \Delta S$. The entropy in each phase satisfies $S = -\partial(V_b F)/\partial T_b$. If r_b is large enough compared to r_h (typically $r_b \gtrsim 1.1 r_h$) then $v_b^T \simeq v_b$, and the difference between the two phases is only due to the fluid free energy, which furthermore vanishes identically in the phase with no black hole. Putting the pieces together and using the chain rule, we derive the latent heat for the transition from the no black hole phase to the black hole phase at a given critical temperature T_c via

$$\ell_b = -T_c \frac{\partial F_{\text{fluid}}}{\partial r_b} \frac{\partial r_b}{\partial T_b} \Big|_{r_{b,c}}. \quad (7.10)$$

7.2.1 Case $\nu < 1$

For $\nu \in [0, 1)$, we have $f_- = 1$ while the other solutions gives $f_+ > 1$ for any value of ν , which is not physical. Therefore $\Delta(T_b)$ cannot change sign as a function of T_b . It satisfies $\Delta(T_b) \leq 0$ for all values of T_b , with $\Delta(T_b) \rightarrow 0$ in the limit of no black hole $r_h \rightarrow 0$, for which $T_b \rightarrow 0$.

We conclude that the black hole phase is energetically favored whenever it exists. The critical temperature is thus $T_c = 0^+$. The latent heat vanishes, hence it is a *second order* phase transition.

The $F(T_b)$ curve is pictured in Fig. 7, left panel.

Case $\nu > 1$

For $\nu \in (1, 2)$, we have $f_+ = 1$ and

$$\sqrt{f_-} = \frac{4 - \nu^2}{\nu^2 + 2}, \quad (7.11)$$

which is inside the $[0, 1]$ interval. There is thus a phase transition at a nonzero value of r_h/r_b ,

$$\frac{r_h}{r_b} \Big|_c = \left(\frac{12(\nu^2 - 1)}{(\nu^2 + 2)^2} \right)^{\frac{1}{4-\nu^2}}. \quad (7.12)$$

The corresponding critical temperature is

$$T_b = \frac{4 - \nu^2}{4} \frac{\eta}{\pi} \left(\frac{(\nu^2 + 2)^2}{12(\nu^2 - 1)} \right)^{\frac{\nu^2 - 1}{4 - \nu^2}} \equiv T_c. \quad (7.13)$$

In terms of the horizon position, it turns out that $\Delta(T_b) > 0$ for $r_h < r_{h,c}$ and $\Delta(T_b) < 0$ for $r_h > r_{h,c}$.

We find a latent heat per unit volume that is finite for any $1 < \nu < 2$,

$$\ell_b = -\frac{12(\nu^2 - 1)}{4 - \nu^2} M_5^3 \eta, \quad (7.14)$$

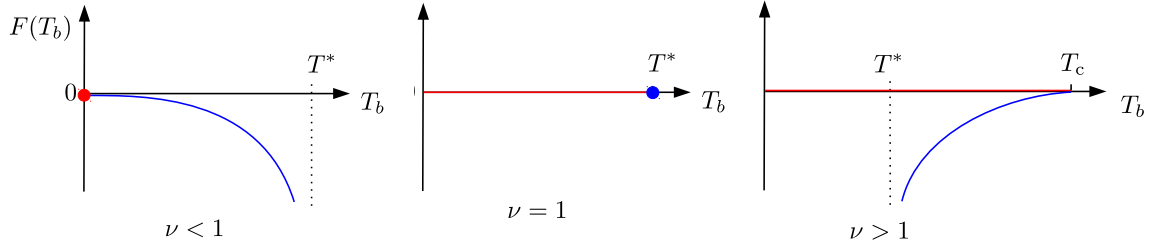


Figure 7. Free energy curves and thermal phases as a function of the temperature of the holographic fluid. Red corresponds to the phase with no black hole, blue corresponds to the black hole phase. The black hole phase is stable at any value of T_b shown on the graph.

therefore the phase transition is *first order*.

Furthermore, the latent heat is *negative*. This is tied to the fact that for $\nu > 1$, T_b decreases when r_b approaches r_h . This implies that there is a cusp in the free energy curve. This is shown in Fig. 7, right panel.

Case $\nu = 1$

For $\nu = 1$ i.e. the linear dilaton background, the fluid has constant temperature $T_b = \frac{3\eta}{4\pi}$ and vanishing free energy, $F_{\text{fluid}} = 0$, as shown in [27, 81]. That is, the fluid has Hagedorn behavior. We conclude that the phase transition occurs at $T_c = \frac{3\eta}{4\pi}$ and is of second order. This is shown in Fig. 7, middle panel.

7.3 Discussion

Heat Capacity

We computed the heat capacity at constant volume of the black hole, which is given by $C_V = -T_b F''(T_b)$. We find that the heat capacity is positive at all values for which the black hole phase is energetically favored. Hence the black hole is thermodynamically stable for all values of ν .

Temperature bound

For $\nu < 1$ and $\nu > 1$ the fluid free energy tends to negative infinity when the black hole approaches the brane. In this limit the temperature approaches the finite value

$$T^* = \frac{4 - \nu^2}{4\pi} \eta. \quad (7.15)$$

For $\nu < 1$, T^* is approached from below, i.e. the fluid temperature is constrained to the interval $T_b \in [0, T^*)$. For $\nu > 1$, T^* is instead approached from above, i.e. the fluid temperature is bounded from below, $T_b \in (T^*, \infty)$. Notice that in the $\nu = 1$ case, the temperature is restricted to the single value T^* .

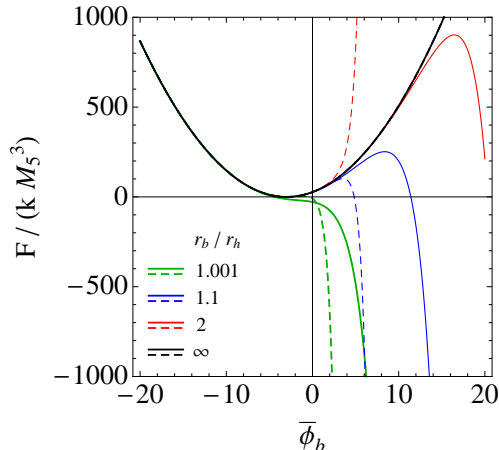


Figure 8. The total free energy density as a function of $\bar{\phi}_b$, assuming the brane-localized effective potential $V_b(\phi_b) = \frac{\gamma}{2}(\phi_b - v_b)^2$. Solid(dashed) lines are for $\nu = 0.5(1.5)$. We have considered $\bar{v}_b = -3$ and $\gamma = 2k$. Unstability of the system occurs when the horizon comes close to the brane.

Cosmological scenario

The thermodynamic behavior of the black hole is perhaps more intuitively understood when considering a brane cosmology-type scenario where a thermal bath of temperature $T \gg T_b$ is present on the brane. The thermal bath leaks energy into the bulk, feeding the bulk black hole, which is assumed not to exist initially. See [106–108] for analyses of such scenarios in AdS. The rigorous evolution of such cosmological scenarios is done using a Vaidya-type metric. Here we discuss them only qualitatively to get a sense of the black hole behavior.

For $\nu < 1$ and $\nu = 1$, the black hole is created via a second order phase transition whenever some energy leaks into the bulk. For $\nu < 1$ the temperature grows while the black hole size increases. For $\nu = 1$ the temperature is instead constant and non zero for any black hole size, since it is independent of r_h .

For $\nu > 1$, the thermal bath should heat up the bulk sufficiently such that a first order phase transition occurs and the black hole directly forms with finite size given by (7.12).⁹ The black hole temperature decreases as its size increases further.

7.4 Instability from Big Black Holes

We study the stability of the brane-dilaton system in the presence of the black hole. This is described by the brane-localized effective potential $U_b(\phi_b)$ given in (7.1). Notice that this is equivalent to study the free energy at $\phi_b \neq v_b$.

The stabilization of ϕ_b is driven by the brane potential $V_b(\phi_b)$, see (6.1). At zero temperature, due to the ϕ_b dependence of η , requiring $U_b''(v_b) > 0$ implies the stability condition $V_b''(v_b) > 2\nu^2\eta$ [81].

⁹The first order phase transition may proceed via bubble nucleation and thus produces gravitational waves, see e.g. [60, 62, 63, 105, 109, 110].

At finite temperature, the extra contribution from the black hole in (7.7) is also proportional to $\eta(\phi_b)$. In the black hole phase this term is negative, since by definition we have $\Delta(r_b, r_h) < 0$ for the black hole phase to be energetically favored.

When the black hole becomes so big that its horizon approaches the brane, $r_h \sim r_b$, the effect of the black hole dominates and we have $\Delta(r_b, r_h) \sim -\frac{4-\nu^2}{6\sqrt{f_b}}$ with f_b approaching zero. Therefore this black hole term tends to *destabilize* the effective potential. The critical value for r_h/r_b depends on the steepness of the U_b potential, and is approximately given by

$$\frac{r_h}{r_b} \approx 1 - \frac{\nu^4}{9} \frac{4 - \nu^2}{(U_b^{0''}(v_b^T))^2} \eta^2(v_b^T). \quad (7.16)$$

Notice that in the stiff potential limit $U_b^{0''} \rightarrow \infty$, the horizon can reach the brane since the potential cannot be destabilized.

We conclude that, for finite $U_b^{0''}$, the T^* temperature cannot be actually reached. A radical change in the system occurs for a value of r_h slightly below r_b : the classical effective potential for ϕ_b becomes unbounded from below — and can only get stabilized at loop level.

Numerical examples of this effect are presented in Fig. 8, where we used $V_b(\phi_b) = \frac{\gamma}{2}(\phi_b - v_b)^2$.

8 Summary

We studied holographic entanglement entropy and revisited thermal phase transitions and confinement in dilaton gravity, with special emphasis on their interplay with bulk curvature singularities.

We mostly focus on a very simple class of backgrounds \mathcal{M}_ν , parameterized by a real parameter ν interpolating between AdS ($\nu = 0$) and linear dilaton ($\nu = 1$) that retains the essence of the phenomena we want to highlight, and also prove some properties in general warped metric. The considered backgrounds are non-asymptotically AdS and feature a flat brane on which the holographic theory is defined. Curvature singularities can be either at infinite or finite conformal distance from the brane. We show that the latter case is automatically implied by a metric zero at finite conformal distance, in which case the singularity acts as a regular boundary that truncates spacetime.

We show that the behaviors of the entanglement, thermodynamics, and confinement properties are all tied to the nature of the bulk singularity. Some important results are summarized in Tab. 1.

Confinement

We first revisit the notion of holographic confinement based on classical strings. In our background the behavior of the string is straightforwardly understood. We show that for $\nu < 1$ ($\nu > 1$) the string bends towards small (large) r , while it is straight for $\nu = 1$. An equivalent coordinate-free statement is that the string living in the \mathcal{M}_ν background is repelled from the string frame curvature singularity.

Value of ν	0 [AdS]	(0, 1)	1 [LD]	(1, 2)	2
Singularity	✗	good			bad
Brane-singularity conf. distance	✗	∞		finite	
Timelike boundary	✗			✓	
Bulk Black hole	✓			✗	
Gravity spectrum ($D \geq 4$)	continuum		gapped cont.	discretum	
Geodesic at fixed Δx	single			double	
Δs^{\max}	∞	finite			
Δx^{\max} (or L_A^{\max})	∞		finite		
Confinement	✗		✓		
Thermal phase transition ($D = 5$)	second order			first order	
Entanglement phase transition	✗		second order	first order	

Table 1. Properties of the \mathcal{M}_ν^- spacetime. From top to bottom, the first block reviews global features, the second block describes brane-to-brane geodesics, and the third block summarizes key holographic properties.

We further show that, when attached to the boundary/brane on which the dual theory is defined, the string is forced to have a straight profile for $\nu > 1$. The resulting picture is that the theory is not confining for $\nu < 1$, while it is perfectly confining for both $\nu = 1$ (linear dilaton) and $\nu > 1$, in each case with the same string tension. We show that this picture provides an intuitive understanding of holographic confinement in asymptotically-AdS backgrounds.

Entanglement Entropy

Having a solid understanding of the confinement criterion, we turn to geodesics and holographic entanglement entropy.

We study the spacelike geodesics of the \mathcal{M}_ν^- spacetime with focus on the brane-to-brane ones. For $\nu \leq 1$ a single geodesic relates two endpoints on the brane while for $\nu > 1$ two geodesics with same endpoint separation exist. We show that for a general warped metric with monotonic coefficients, this doubling phenomenon is tied to the existence of a singularity at finite conformal distance.

We derive approximate formulas for geodesic distances in the generic dilaton gravity background. We also prove an exact general formula for the geodesic distance in the linear dilaton background. The linear dilaton distance formula has remarkable properties, including that spacelike distances are bounded from above.

In our dilaton gravity background, we find that the brane-to-brane distance (Δx) is bounded from above when $\nu \geq 1$. The shorter path between two points with larger endpoint separation is the one that goes straight to the singularity — on which distances vanish. The geodesics tend asymptotically to this “square” path when their tip approaches the singularity.

Building on these results we explore the holographic entanglement entropy of a space-

like $d - 1$ strip localized on the brane, applying the Ryu-Takayanagi formula. Two surfaces anchored to the brane are possible: a smooth surface and a square one that reaches the singularity.

Working with the general warped metric, we first show that a metric zero at finite conformal distance implies that the square surface has finite area and ends on a curvature singularity. Assuming monotonous metric coefficients, we further show that the possibility of a HEE phase transition is tied to the existence of a singularity at finite conformal distance, and determine a sufficient condition for the HEE phase transition to occur. We further show that for such a singularity, there exist necessarily two smooth surfaces of different areas anchored to a same $(d - 1)$ -strip on the brane.

These phenomena are explicitly shown to occur in the \mathcal{M}_ν^- background. For $\nu < 1$ the smooth surface has minimal area for any width of the strip. In this case the entanglement entropy reaches a plateau at large strip width for $\nu \geq 0$ if $d > 2$ and for $\nu > 0$ if $d = 2$. The existence of HEE plateaux has been noted in the literature at finite temperature [94], here the plateau appears at zero temperature.

For $\nu = 1$, the entanglement entropy features a transition between the smooth surface and the square surface at finite strip width. From our general analysis (and also from our exact formula for the linear dilaton geodesics distance) we find that a discontinuity occurs at second order. Hence the linear dilaton stands out once again as a special, critical case.

For $\nu > 1$, there are two smooth surfaces and the square one. A transition between the smooth surface of smaller area and the square surface occurs at finite strip width. The transition turns out to be of first order. The behavior of the areas, and of the transition, resembles the ones obtained in stringy setups in [64, 71, 73, 75]. In our setup we find that this characteristic behavior is tied to the curvature singularity being at finite conformal distance.

Thermodynamics and Stability

We compute the on-shell effective action of the system with no black hole (i.e. at zero temperature) as a function of the classical value of the dilaton field and of the brane position. Upon gauge fixing of spacetime fluctuations, the scalar fluctuations reduce to a single degree of freedom, the radion. We derive the radion profile and compute the full quadratic action of the radion, which completes and cross checks the results from [81]. Under a certain condition on the brane-localized potential, the radion is massive, which ensures stability of the system. The radion quadratic action would be needed to compute corrections to black hole entropy or to the HEE [95, 97, 98, 100].

The existence of the planar black hole amounts, from the viewpoint of the brane, to the existence of a perfect fluid. We study the thermodynamics of this fluid, including phase transitions, extending the results from [81].

We show that for $\nu \leq 1$ the fluid/black hole appears via a second order phase transition whenever the temperature is nonzero. In contrast, for $\nu > 1$, the black hole appears above a nonzero critical temperature via a first order phase transition. In the linear dilaton case $\nu = 1$, the black hole has always the same nonzero temperature, but appears via a second order phase transition.

Remarkably, the order of these thermal phase transitions matches the one of the entanglement entropy phase transitions.

In the black hole phase considered, the black hole is always thermodynamically stable in the sense of having positive heat capacity. The black hole temperature increases with its size for $\nu < 1$, while it decreases with its size for $\nu > 1$, which causes the latent heat to be negative. The black hole temperature admits an upper bound for $\nu < 1$ and a lower bound for $\nu > 1$, which is tied to the brane not being engulfed by the horizon.

We demonstrate that, in the extreme situation where the horizon approaches the brane, a dramatic instability in the dilaton vev occurs, that makes the classical effective potential unbounded from below.

Acknowledgments

We thank Lucas de Souza for insightful comments regarding App. A. The work of EM is supported by the project PID2020-114767GB-I00 and by the Ramón y Cajal Program under Grant RYC-2016-20678 funded by MCIN/AEI/10.13039/501100011033 and by “FSE Investing in your future”, by Junta de Andalucía under Grant FQM-225, and by the “Prórrogas de Contratos Ramón y Cajal” Program of the University of Granada. The work of MQ is partly supported by Spanish MICIN under Grant PID2020-115845GB-I00, and by the Catalan Government under Grant 2021SGR00649. IFAE is partially funded by the CERCA program of the Generalitat de Catalunya.

A Derivation of Property (2.10)

We prove Prop. (2.10). The essence of the derivation is to show that, using the mean value theorem, any interval in the vicinity of the metric zero contains a point such that $a'(z)/a(z)$ is singular, no matter how small the interval is. We make the hypothesis that $a'(z)/a(z)$ is *strictly monotonous* near the singularity.

The mean value theorem states that for any function $a(z)$ continuous on $[z_1, z_2]$ and differentiable on (z_1, z_2) there is at least one point z_{12} in (z_1, z_2) such that

$$\log a(z_2) - \log a(z_1) = \frac{a'(z_{12})}{a(z_{12})}(z_2 - z_1). \quad (\text{A.1})$$

We apply the theorem in the vicinity of the metric zero, $a(z_s) = 0$. Following the convention from section 5.2, spacetime is defined to the right of z_s , $z \geq z_s$. We place the small closed interval to the right of the metric zero, and take the limit $z_1 \rightarrow z_s^+$ in (A.1).

To ensure that z_{12} converges when taking the limit $z_1 \rightarrow z_s^+$, we implement this limit using a discrete sequence as follows. Define $z_1 \equiv z_s + \frac{1}{n}$, where $n \in \mathbb{N}$ starts at a value larger than $\frac{1}{z_2 - z_s}$ and is taken to infinity. For each n there is a value of z_{12} , denoted $z_{12} \equiv z(n, z_2) = z_n$. Since $z_n \in (z_s, z_2)$, (z_n) is a bounded sequence. Thus the Bolzano-Weierstrass theorem ensures that there exists a subsequence $(z_{n_j}) \equiv (\hat{z}_j)$ of (z_n) that is convergent, i.e. $\lim_{j \rightarrow \infty} \hat{z}_j = \hat{z}$, with $\hat{z} = \hat{z}(z_2)$.

Starting from (A.1), we have

$$\lim_{j \rightarrow \infty} \frac{a'(\hat{z}_j)}{a(\hat{z}_j)} = \lim_{z \rightarrow \hat{z}} \frac{a'(z)}{a(z)} = \lim_{j \rightarrow \infty} \frac{\log a(z_2) - \log a(z_s + n_j^{-1})}{z_2 - z_s - n_j^{-1}} = \infty, \quad (\text{A.2})$$

since $\log(a(z))$ diverges at z_s while by assumption z_s is finite. That is, there is at least one point \hat{z} in (z_s, z_2) for which $a'(z)/a(z)$ is infinite. The assumption that $a'(z)/a(z)$ is strictly monotonous on the interval (z_s, z_2) implies that $\log(a(z))$ is strictly concave or convex, which ensures that the intermediate point \hat{z} is unique.

We can then approach z_2 to z_s^+ , such that the intermediate point $\hat{z}(z_2)$ is forced to tend to z_s^+ . Taking this limit in (A.2), we obtain

$$\lim_{z_2 \rightarrow z_s^+} \frac{a'(\hat{z}(z_2))}{a(\hat{z}(z_2))} = \lim_{\hat{z} \rightarrow z_s^+} \frac{a'(\hat{z})}{a(\hat{z})} = \infty. \quad (\text{A.3})$$

This proves Prop. (2.10).

B Geodesic Distances

B.1 Anti-de Sitter Spacetime

AdS is \mathcal{M}_ν^- with $\nu = 0$. The geodesic equations in that case are

$$r(s) = r_0 \cosh(\eta s), \quad (\text{B.1})$$

$$x^\mu(s) = \frac{U^\mu L^2}{\eta r_0^2} \tanh(\eta s). \quad (\text{B.2})$$

Squaring the above equations it follows directly that spacelike geodesics in AdS_{d+1} obeys a $d + 1$ -dimensional ellipsoid equation with $z = 1/r$,

$$r_0^2 z^2 + \frac{r_0^2}{L^2} \eta^2 \eta_{\mu\nu} x^\mu x^\nu = 1. \quad (\text{B.3})$$

The spatial distance between two points is found to be

$$\Delta s = \frac{2}{\eta} \operatorname{arcsinh} \sqrt{\frac{(\Delta r)^2}{4r_1 r_2} + \frac{\eta^2 r_1 r_2}{4L^2} (\Delta x)^2}. \quad (\text{B.4})$$

For a path with $r_1 = r_2 = r_b$ that does not reaches $r = 0$, this reduces to

$$\Delta s = \frac{2}{\eta} \operatorname{arcsinh} \left(\frac{\eta r_b}{2L} \Delta x \right). \quad (\text{B.5})$$

For any path that reaches $r = 0$, we have $\Delta s \rightarrow \infty$.

B.2 \mathcal{M}_ν^- Spacetime with No Black Hole

Equations (4.4) and (4.5) are exact solutions for spacelike geodesics in \mathcal{M}_ν^- with no black hole. From these solutions we find good approximations for the brane-to-brane geodesic lengths.

B.2.1 Case $r_0 \ll r_b$

For geodesics that go far from the brane, $r_0 \ll r_b$, the geodesic length $\Delta s = 2|s(r = r_b) - s(r = r_0)|$ is approximately

$$\Delta s \simeq \frac{2}{\eta\nu^2} + \frac{3r_0^4}{4\eta r_b^4(\nu^2 - 4)} + \frac{r_0^2}{\eta r_b^2(\nu^2 - 2)} + \frac{\sqrt{\pi} \left(\frac{r_0}{r_b}\right)^{\nu^2} \Gamma\left(-\frac{\nu^2}{2}\right)}{\eta \Gamma\left(\frac{1}{2}(1 - \nu^2)\right)}, \quad (\text{B.6})$$

for $\nu \neq 1, \sqrt{2}, 2$. Such special cases can be solved exactly.

Doing the same expansion for the spacelike Minkowski distance of the endpoints $\Delta x = \sqrt{(\Delta x^\mu)^2}$, we find

$$\Delta x \simeq \frac{2Lr_0}{\eta r_b^2(\nu^2 - 2)} + \frac{\sqrt{\pi} L \left(\frac{r_0}{r_b}\right)^{\nu^2} \Gamma\left(1 - \frac{\nu^2}{2}\right)}{\eta r_0 \Gamma\left(\frac{1}{2}(3 - \nu^2)\right)}, \quad (\text{B.7})$$

for $\nu \neq \sqrt{2}, \sqrt{3}$. With the expression above, we find r_0 and write Δs in function of Δx . At first order, we obtain (4.8) and (4.9).

In the case of $\nu > 1$, these approximations correspond to the long geodesics, see Fig. 4.

B.2.2 Case $r_0 \sim r_b$

For a geodesic that stays near the brane, $r_0 \sim r_b$, a better approximation is

$$\Delta s \simeq \frac{2}{\eta} \left(\frac{r_0}{r_b}\right)^{\nu^2} \sqrt{2 \left(\frac{r_b}{r_0} - 1\right)}, \quad (\text{B.8})$$

$$\Delta x \simeq \frac{2L}{\eta r_0} \left(\frac{r_0}{r_b}\right)^{\nu^2} \sqrt{2 \left(\frac{r_b}{r_0} - 1\right)}. \quad (\text{B.9})$$

There is thus a linear relation $\Delta s = \frac{r_0}{L} \Delta x$. At first order approximation this reproduces (4.7). In the case of $\nu > 1$, these approximations correspond to the short geodesics, see Fig. 4.

B.3 \mathcal{M}_ν^- Spacetime with a Black Hole

Equations (4.10) and (4.11) cannot be solved analytically for arbitrary ν . However, we can make some approximations.

B.3.1 Case $r_0 \gg r_h$

For brane-to-brane geodesics with r_0 the tip of the geodesic, having $r_0 \gg r_h$ implies $r_h \ll r$. In that limit, the presence of the black hole horizon induces a small correction to

the geodesics. We expand (4.10),

$$s_{\text{b.h.}}(r) \simeq \frac{1}{r_b^{\nu^2} \eta} \int dr \frac{r^{\nu^2-1}}{\left(1 - \frac{1}{2} \left(\frac{r_h}{r}\right)^{4-\nu^2}\right) \sqrt{1 - \frac{r_0^2}{r^2}}} \quad (\text{B.10})$$

$$\simeq \frac{1}{r_b^{\nu^2} \eta} \int dr \frac{r^{\nu^2-1}}{\sqrt{1 - \frac{r_0^2}{r^2}}} \left(1 + \frac{1}{2} \left(\frac{r_h}{r}\right)^{4-\nu^2} + \dots\right). \quad (\text{B.11})$$

The first term in (B.11) is the solution with no black hole, defined in (4.4). The second term is the black hole-induced correction, that can be also obtained from (4.4) if one substitutes the ν parameter with $\nu^2 \rightarrow 2(\nu^2 - 2)$, such that

$$s_{\text{b.h.}}(r) \simeq s|_{\nu^2} + \frac{1}{2} (r_h r_b)^{4-\nu^2} s|_{\nu^2 \rightarrow 2(\nu^2-2)} + \dots \quad (\text{B.12})$$

The same applies for (4.11),

$$x_{\text{b.h.}}^\mu \simeq x^\mu|_{\nu^2} + \frac{1}{2} (r_h r_b)^{4-\nu^2} x^\mu|_{\nu^2 \rightarrow 2(\nu^2-2)} + \dots, \quad (\text{B.13})$$

where $x^\mu|_{\nu^2}$ is defined in (4.5). The black hole-induced corrections can then be evaluated using the approximations given in sections B.2.1 and B.2.2, or solving exactly for special values of ν . For example, if $\nu^2 = 5/2$, the correction term is proportional to the geodesic distance in linear dilaton spacetime, $\nu = 1$. For $\nu^2 = 2$, the correction term is proportional to the distance in AdS, $\nu = 0$.

B.3.2 Case $r_0 \ll r_h$

For $r_h > r_0$, we have $r \gg r_0$ along all the path, allowing us to approximate (4.10) as

$$s_{\text{b.h.}} \simeq \frac{1}{r_b^{\nu^2} \eta} \int dr \frac{r^{\nu^2-1}}{\sqrt{1 - \left(\frac{r_h}{r}\right)^{4-\nu^2}}}. \quad (\text{B.14})$$

This can be computed exactly, giving the solutions

$$s_{\text{b.h.}} = \begin{cases} \frac{1}{2\eta} \log(r^2 + \sqrt{r^4 - r_h^4}) + \text{cst}, & \nu = 0 \\ \frac{r^{\nu^2}}{r_b^{\nu^2} \eta \nu^2} \times {}_2F_1\left(\frac{1}{2}, \frac{\nu^2}{\nu^2-4}; 1 + \frac{\nu^2}{\nu^2-4}; \left(\frac{r_h}{r}\right)^{4-\nu^2}\right) + \text{cst}, & \nu \neq 0 \end{cases}. \quad (\text{B.15})$$

This leads to the result (4.12) when taking $r_b \gg r_h$.

References

- [1] O. Aharony, S. S. Gubser, J. M. Maldacena, H. Ooguri, and Y. Oz, *Large N field theories, string theory and gravity*, Phys. Rept. **323** (2000) 183–386, [[hep-th/9905111](#)].
- [2] A. Zaffaroni, *Introduction to the AdS-CFT correspondence*, Class. Quant. Grav. **17** (2000) 3571–3597.

- [3] J. Kaplan, “Lectures on AdS/CFT from the Bottom Up.” <https://sites.krieger.jhu.edu/jared-kaplan/files/2016/05/AdSCFTCourseNotesCurrentPublic.pdf>.
- [4] H. Nastase, *Introduction to AdS-CFT*, [arXiv:0712.0689](https://arxiv.org/abs/0712.0689).
- [5] J. Polchinski and M. J. Strassler, *Hard scattering and gauge / string duality*, Phys. Rev. Lett. **88** (2002) 031601, [[hep-th/0109174](https://arxiv.org/abs/hep-th/0109174)].
- [6] J. Erlich, E. Katz, D. T. Son, and M. A. Stephanov, *QCD and a holographic model of hadrons*, Phys. Rev. Lett. **95** (2005) 261602, [[hep-ph/0501128](https://arxiv.org/abs/hep-ph/0501128)].
- [7] L. Da Rold and A. Pomarol, *Chiral symmetry breaking from five dimensional spaces*, Nucl. Phys. B **721** (2005) 79–97, [[hep-ph/0501218](https://arxiv.org/abs/hep-ph/0501218)].
- [8] U. Gursoy and E. Kiritsis, *Exploring improved holographic theories for QCD: Part I*, JHEP **02** (2008) 032, [[arXiv:0707.1324](https://arxiv.org/abs/0707.1324)].
- [9] U. Gursoy, E. Kiritsis, and F. Nitti, *Exploring improved holographic theories for QCD: Part II*, JHEP **02** (2008) 019, [[arXiv:0707.1349](https://arxiv.org/abs/0707.1349)].
- [10] O. Aharony, *A Brief review of ‘little string theories’*, Class. Quant. Grav. **17** (2000) 929–938, [[hep-th/9911147](https://arxiv.org/abs/hep-th/9911147)].
- [11] D. Kutasov, *Introduction to little string theory*, ICTP Lect. Notes Ser. **7** (2002) 165–209.
- [12] I. Antoniadis, C. Markou, and F. Rondeau, *Aspects of compactification on a linear dilaton background*, JHEP **09** (2021) 137, [[arXiv:2106.15184](https://arxiv.org/abs/2106.15184)].
- [13] N. Seiberg, *New theories in six-dimensions and matrix description of M theory on T^{**5} and $T^{**5}/Z(2)$* , Phys. Lett. B **408** (1997) 98–104, [[hep-th/9705221](https://arxiv.org/abs/hep-th/9705221)].
- [14] M. Berkooz, M. Rozali, and N. Seiberg, *Matrix description of M theory on T^{**4} and T^{**5}* , Phys. Lett. B **408** (1997) 105–110, [[hep-th/9704089](https://arxiv.org/abs/hep-th/9704089)].
- [15] A. Giveon, N. Itzhaki, and D. Kutasov, *$T\bar{T}$ and LST*, JHEP **07** (2017) 122, [[arXiv:1701.05576](https://arxiv.org/abs/1701.05576)].
- [16] G. Giribet, *$T\bar{T}$ -deformations, AdS/CFT and correlation functions*, JHEP **02** (2018) 114, [[arXiv:1711.02716](https://arxiv.org/abs/1711.02716)].
- [17] M. Asrat, A. Giveon, N. Itzhaki, and D. Kutasov, *Holography Beyond AdS*, Nucl. Phys. B **932** (2018) 241–253, [[arXiv:1711.02690](https://arxiv.org/abs/1711.02690)].
- [18] T. Araujo, E. O. Colgáin, Y. Sakatani, M. M. Sheikh-Jabbari, and H. Yavartanoo, *Holographic integration of $T\bar{T} \setminus \mathcal{E} J\bar{T}$ via $O(d, d)$* , JHEP **03** (2019) 168, [[arXiv:1811.03050](https://arxiv.org/abs/1811.03050)].
- [19] S. Chakraborty, G. Katoch, and S. R. Roy, *Holographic complexity of LST and single trace $T\bar{T}$* , JHEP **03** (2021) 275, [[arXiv:2012.11644](https://arxiv.org/abs/2012.11644)].
- [20] S. Chakraborty, *$\frac{SL(2, \mathbb{R}) \times U(1)}{U(1)}$ CFT, NS5+F1 system and single trace $T\bar{T}$* , JHEP **03** (2021) 113, [[arXiv:2012.03995](https://arxiv.org/abs/2012.03995)].
- [21] S. Georgescu and M. Guica, *Infinite $T\bar{T}$ -like symmetries of compactified LST*, [arXiv:2212.09768](https://arxiv.org/abs/2212.09768).
- [22] M. Guica, “ $T\bar{T}$ deformations and holography.” <https://indi.to/h333c>.
- [23] C.-K. Chang, C. Ferko, and S. Sethi, *Holography and irrelevant operators*, Phys. Rev. D **107** (2023), no. 12 126021, [[arXiv:2302.03041](https://arxiv.org/abs/2302.03041)].

- [24] S. Chakraborty, A. Giveon, and D. Kutasov, *Comments on single-trace $T\bar{T}$ holography*, JHEP **06** (2023) 018, [[arXiv:2303.12422](#)].
- [25] S. Chakraborty, A. Giveon, and D. Kutasov, *Momentum in Single-trace $T\bar{T}$ Holography*, [[arXiv:2304.09212](#)].
- [26] O. Aharony and N. Barel, *Correlation functions in $T\bar{T}$ -deformed Conformal Field Theories*, JHEP **08** (2023) 035, [[arXiv:2304.14091](#)].
- [27] S. Fichet, E. Megías, and M. Quirós, *Holography of Linear Dilaton Spacetimes from the Bottom Up*, Phys. Rev. D **109** (2024), no. 10 106011, [[arXiv:2309.02489](#)].
- [28] I. Antoniadis, S. Dimopoulos, and A. Giveon, *Little string theory at a TeV*, JHEP **05** (2001) 055, [[hep-th/0103033](#)].
- [29] I. Antoniadis, A. Arvanitaki, S. Dimopoulos, and A. Giveon, *Phenomenology of TeV Little String Theory from Holography*, Phys. Rev. Lett. **108** (2012) 081602, [[arXiv:1102.4043](#)].
- [30] C. Csáki, G. Lee, S. J. Lee, S. Lombardo, and O. Telem, *Continuum Naturalness*, JHEP **03** (2019) 142, [[arXiv:1811.06019](#)].
- [31] E. Megías and M. Quirós, *Gapped Continuum Kaluza-Klein spectrum*, JHEP **08** (2019) 166, [[arXiv:1905.07364](#)].
- [32] E. Megías and M. Quirós, *The Continuum Linear Dilaton*, Acta Phys. Polon. B **52** (2021) 711, [[arXiv:2104.10260](#)].
- [33] E. Megías and M. Quirós, *Analytical Green's functions for continuum spectra*, JHEP **09** (2021) 157, [[arXiv:2106.09598](#)].
- [34] S. Fichet, E. Megías, and M. Quirós, *Continuum effective field theories, gravity, and holography*, Phys. Rev. D **107** (2023), no. 9 096016, [[arXiv:2208.12273](#)].
- [35] S. Fichet, E. Megías, and M. Quirós, *Cosmological dark matter from a bulk black hole*, Phys. Rev. D **107** (2023), no. 11 115014, [[arXiv:2212.13268](#)].
- [36] G. 't Hooft, *Dimensional reduction in quantum gravity*, Conf. Proc. C **930308** (1993) 284–296, [[gr-qc/9310026](#)].
- [37] L. Susskind, *The World as a hologram*, J. Math. Phys. **36** (1995) 6377–6396, [[hep-th/9409089](#)].
- [38] G. 't Hooft, *The Holographic principle: Opening lecture*, Subnucl. Ser. **37** (2001) 72–100, [[hep-th/0003004](#)].
- [39] R. Bousso, *A Covariant entropy conjecture*, JHEP **07** (1999) 004, [[hep-th/9905177](#)].
- [40] R. Bousso, *The Holographic principle*, Rev. Mod. Phys. **74** (2002) 825–874, [[hep-th/0203101](#)].
- [41] A. Karch, E. Katz, D. T. Son, and M. A. Stephanov, *Linear confinement and AdS/QCD*, Phys. Rev. **D74** (2006) 015005, [[hep-ph/0602229](#)].
- [42] B. Batell and T. Gherghetta, *Dynamical Soft-Wall AdS/QCD*, Phys. Rev. **D78** (2008) 026002, [[arXiv:0801.4383](#)].
- [43] P. Colangelo, F. De Fazio, F. Giannuzzi, F. Jugeau, and S. Nicotri, *Light scalar mesons in the soft-wall model of AdS/QCD*, Phys. Rev. D **78** (2008) 055009, [[arXiv:0807.1054](#)].
- [44] J. A. Cabrer, G. von Gersdorff, and M. Quirós, *Soft-Wall Stabilization*, New J. Phys. **12** (2010) 075012, [[arXiv:0907.5361](#)].

- [45] G. von Gersdorff, *From Soft Walls to Infrared Branes*, Phys. Rev. **D82** (2010) 086010, [[arXiv:1005.5134](#)].
- [46] E. Megías and M. Valle, *Singular perturbation theory for the thermodynamic properties of holographic QCD*, Fortsch. Phys. **66** (2018), no. 7 1800035, [[arXiv:1707.04747](#)].
- [47] E. Witten, *Branes and the dynamics of QCD*, Nucl. Phys. B **507** (1997) 658–690, [[hep-th/9706109](#)].
- [48] A. Hanany, M. J. Strassler, and A. Zaffaroni, *Confinement and strings in MQCD*, Nucl. Phys. B **513** (1998) 87–118, [[hep-th/9707244](#)].
- [49] J. M. Maldacena, *Wilson loops in large N field theories*, Phys. Rev. Lett. **80** (1998) 4859–4862, [[hep-th/9803002](#)].
- [50] Y. Kinar, E. Schreiber, and J. Sonnenschein, *Precision ‘measurements’ of the Q anti-Q potential in MQCD*, Nucl. Phys. B **544** (1999) 633–649, [[hep-th/9809133](#)].
- [51] A. M. Polyakov, *The Wall of the cave*, Int. J. Mod. Phys. A **14** (1999) 645–658, [[hep-th/9809057](#)].
- [52] S.-J. Rey and J.-T. Yee, *Macroscopic strings as heavy quarks in large N gauge theory and anti-de Sitter supergravity*, Eur. Phys. J. C **22** (2001) 379–394, [[hep-th/9803001](#)].
- [53] O. Andreev and V. I. Zakharov, *Heavy-quark potentials and AdS/QCD*, Phys. Rev. D **74** (2006) 025023, [[hep-ph/0604204](#)].
- [54] O. Andreev and V. I. Zakharov, *On Heavy-Quark Free Energies, Entropies, Polyakov Loop, and AdS/QCD*, JHEP **04** (2007) 100, [[hep-ph/0611304](#)].
- [55] B. Galow, E. Megías, J. Nian, and H. J. Pirner, *Phenomenology of AdS/QCD and Its Gravity Dual*, Nucl. Phys. B **834** (2010) 330–362, [[arXiv:0911.0627](#)].
- [56] N. Horigome and Y. Tanii, *Holographic chiral phase transition with chemical potential*, JHEP **01** (2007) 072, [[hep-th/0608198](#)].
- [57] U. Gursoy, E. Kiritsis, L. Mazzanti, and F. Nitti, *Holography and Thermodynamics of 5D Dilaton-gravity*, JHEP **05** (2009) 033, [[arXiv:0812.0792](#)].
- [58] T. Konstandin, G. Nardini, and M. Quirós, *Gravitational Backreaction Effects on the Holographic Phase Transition*, Phys. Rev. D **82** (2010) 083513, [[arXiv:1007.1468](#)].
- [59] E. Megías, H. J. Pirner, and K. Veschgini, *QCD thermodynamics using five-dimensional gravity*, Phys. Rev. D **83** (2011) 056003, [[arXiv:1009.2953](#)].
- [60] E. Megías, G. Nardini, and M. Quirós, *Cosmological Phase Transitions in Warped Space: Gravitational Waves and Collider Signatures*, JHEP **09** (2018) 095, [[arXiv:1806.04877](#)].
- [61] E. Megías, G. Nardini, and M. Quirós, *Gravitational Imprints from Heavy Kaluza-Klein Resonances*, Phys. Rev. D **102** (2020), no. 5 055004, [[arXiv:2005.04127](#)].
- [62] E. Megías, G. Nardini, and M. Quirós, *Pulsar timing array stochastic background from light Kaluza-Klein resonances*, Phys. Rev. D **108** (2023), no. 9 095017, [[arXiv:2306.17071](#)].
- [63] R. K. Mishra and L. Randall, *Phase Transition to RS: Cool, not Supercool*, [[arXiv:2401.09633](#)].
- [64] I. R. Klebanov, D. Kutasov, and A. Murugan, *Entanglement as a probe of confinement*, Nucl. Phys. B **796** (2008) 274–293, [[arXiv:0709.2140](#)].

- [65] I. Bah, A. Faraggi, L. A. Pando Zayas, and C. A. Terrero-Escalante, *Holographic entanglement entropy and phase transitions at finite temperature*, Int. J. Mod. Phys. A **24** (2009) 2703–2728, [[arXiv:0710.5483](#)].
- [66] M. Fujita, T. Nishioka, and T. Takayanagi, *Geometric Entropy and Hagedorn/Deconfinement Transition*, JHEP **09** (2008) 016, [[arXiv:0806.3118](#)].
- [67] N. Engelhardt and G. T. Horowitz, *Entanglement Entropy Near Cosmological Singularities*, JHEP **06** (2013) 041, [[arXiv:1303.4442](#)].
- [68] S. Chakraborty, A. Giveon, N. Itzhaki, and D. Kutasov, *Entanglement beyond AdS*, Nucl. Phys. B **935** (2018) 290–309, [[arXiv:1805.06286](#)].
- [69] M. Fujita, S. He, and Y. Sun, *Thermodynamical property of entanglement entropy and deconfinement phase transition*, Phys. Rev. D **102** (2020), no. 12 126019, [[arXiv:2005.01048](#)].
- [70] R. da Rocha, *Holographic entanglement entropy, deformed black branes, and deconfinement in AdS/QCD*, Phys. Rev. D **105** (2022), no. 2 026014, [[arXiv:2111.01244](#)].
- [71] N. Jokela, H. Ruotsalainen, and J. G. Subils, *Limitations of entanglement entropy in detecting thermal phase transitions*, [arXiv:2310.11205](#).
- [72] U. Kol, C. Nunez, D. Schofield, J. Sonnenschein, and M. Warschawski, *Confinement, Phase Transitions and non-Locality in the Entanglement Entropy*, JHEP **06** (2014) 005, [[arXiv:1403.2721](#)].
- [73] N. Jokela and J. G. Subils, *Is entanglement a probe of confinement?*, JHEP **02** (2021) 147, [[arXiv:2010.09392](#)].
- [74] S. Griener, D. E. Kharzeev, and I. Zahed, *Entanglement entropy in a time-dependent holographic Schwinger pair creation*, Phys. Rev. D **108** (2023), no. 12 126014, [[arXiv:2310.12042](#)].
- [75] A. Fatemiabhari and C. Nunez, *From conformal to confining field theories using holography*, [arXiv:2401.04158](#).
- [76] J. Abajo-Arastia, J. Aparicio, and E. Lopez, *Holographic Evolution of Entanglement Entropy*, JHEP **11** (2010) 149, [[arXiv:1006.4090](#)].
- [77] A. Bagchi, R. Basu, D. Grumiller, and M. Riegler, *Entanglement entropy in Galilean conformal field theories and flat holography*, Phys. Rev. Lett. **114** (2015), no. 11 111602, [[arXiv:1410.4089](#)].
- [78] J. Erdmenger, D. Fernandez, M. Flory, E. Megías, A.-K. Straub, and P. Witkowski, *Time evolution of entanglement for holographic steady state formation*, JHEP **10** (2017) 034, [[arXiv:1705.04696](#)].
- [79] J. Casalderrey-Solana, C. Ecker, D. Mateos, and W. Van Der Schee, *Strong-coupling dynamics and entanglement in de Sitter space*, JHEP **03** (2021) 181, [[arXiv:2011.08194](#)].
- [80] Z. Li, *Universality of holographic entanglement properties in holographic QCD*, [arXiv:2402.02944](#).
- [81] S. Fichet, E. Megías, and M. Quirós, *Holographic Fluids from 5D Dilaton Gravity*, [arXiv:2311.14233](#).
- [82] G. K. Karananas, A. Kehagias, and J. Taskas, *Islands in linear dilaton black holes*, JHEP **03** (2021) 253, [[arXiv:2101.00024](#)].

- [83] S. S. Gubser, *Curvature singularities: The Good, the bad, and the naked*, Adv. Theor. Math. Phys. **4** (2000) 679–745, [[hep-th/0002160](#)].
- [84] Y. Kinar, E. Schreiber, and J. Sonnenschein, *Q anti-Q potential from strings in curved space-time: Classical results*, Nucl. Phys. B **566** (2000) 103–125, [[hep-th/9811192](#)].
- [85] E. S. Fradkin and A. A. Tseytlin, *Quantum String Theory Effective Action*, Nucl. Phys. B **261** (1985) 1–27. [Erratum: Nucl.Phys.B 269, 745–745 (1986)].
- [86] C. G. Callan, Jr., E. J. Martinec, M. J. Perry, and D. Friedan, *Strings in Background Fields*, Nucl. Phys. B **262** (1985) 593–609.
- [87] C. Lovelace, *Stability of String Vacua. 1. A New Picture of the Renormalization Group*, Nucl. Phys. B **273** (1986) 413–467.
- [88] M. Blau, “Lectures on Quantum Gravity and Black Holes.”
<http://www.hartmanhep.net/topics2015/gravity-lectures.pdf>.
- [89] S. Ryu and T. Takayanagi, *Holographic derivation of entanglement entropy from AdS/CFT*, Phys. Rev. Lett. **96** (2006) 181602, [[hep-th/0603001](#)].
- [90] T. Nishioka, S. Ryu, and T. Takayanagi, *Holographic Entanglement Entropy: An Overview*, J. Phys. A **42** (2009) 504008, [[arXiv:0905.0932](#)].
- [91] H. Casini, M. Huerta, and R. C. Myers, *Towards a derivation of holographic entanglement entropy*, JHEP **05** (2011) 036, [[arXiv:1102.0440](#)].
- [92] M. Headrick, *General properties of holographic entanglement entropy*, JHEP **03** (2014) 085, [[arXiv:1312.6717](#)].
- [93] D. D. Blanco, H. Casini, L.-Y. Hung, and R. C. Myers, *Relative Entropy and Holography*, JHEP **08** (2013) 060, [[arXiv:1305.3182](#)].
- [94] V. E. Hubeny, H. Maxfield, M. Rangamani, and E. Tonni, *Holographic entanglement plateaux*, JHEP **08** (2013) 092, [[arXiv:1306.4004](#)].
- [95] T. Faulkner, A. Lewkowycz, and J. Maldacena, *Quantum corrections to holographic entanglement entropy*, JHEP **11** (2013) 074, [[arXiv:1307.2892](#)].
- [96] A. Lewkowycz and J. Maldacena, *Generalized gravitational entropy*, JHEP **08** (2013) 090, [[arXiv:1304.4926](#)].
- [97] T. Barrella, X. Dong, S. A. Hartnoll, and V. L. Martin, *Holographic entanglement beyond classical gravity*, JHEP **09** (2013) 109, [[arXiv:1306.4682](#)].
- [98] N. Engelhardt and A. C. Wall, *Quantum Extremal Surfaces: Holographic Entanglement Entropy beyond the Classical Regime*, JHEP **01** (2015) 073, [[arXiv:1408.3203](#)].
- [99] H. Araki and E. H. Lieb, *Entropy inequalities*, Commun. Math. Phys. **18** (1970) 160–170.
- [100] D. V. Fursaev and S. N. Solodukhin, *On one loop renormalization of black hole entropy*, Phys. Lett. B **365** (1996) 51–55, [[hep-th/9412020](#)].
- [101] C. Csaki, M. L. Graesser, and G. D. Kribs, *Radion dynamics and electroweak physics*, Phys. Rev. D **63** (2001) 065002, [[hep-th/0008151](#)].
- [102] S. Fichtel, *On holography in general background and the boundary effective action from AdS to dS*, JHEP **07** (2022) 113, [[arXiv:2112.00746](#)].

- [103] R. B. Mann and R. McNees, *Boundary Terms Unbound! Holographic Renormalization of Asymptotically Linear Dilaton Gravity*, Class. Quant. Grav. **27** (2010) 065015, [[arXiv:0905.3848](#)].
- [104] T. Shiromizu, K.-i. Maeda, and M. Sasaki, *The Einstein equation on the 3-brane world*, Phys. Rev. D **62** (2000) 024012, [[gr-qc/9910076](#)].
- [105] P. Creminelli, A. Nicolis, and R. Rattazzi, *Holography and the electroweak phase transition*, JHEP **03** (2002) 051, [[hep-th/0107141](#)].
- [106] D. Langlois, L. Sorbo, and M. Rodriguez-Martinez, *Cosmology of a brane radiating gravitons into the extra dimension*, Phys. Rev. Lett. **89** (2002) 171301, [[hep-th/0206146](#)].
- [107] D. Langlois and L. Sorbo, *Bulk gravitons from a cosmological brane*, Phys. Rev. D **68** (2003) 084006, [[hep-th/0306281](#)].
- [108] S. S. Gubser, I. R. Klebanov, and A. M. Polyakov, *Gauge theory correlators from noncritical string theory*, Phys. Lett. **B428** (1998) 105–114, [[hep-th/9802109](#)].
- [109] P. Baratella, A. Pomarol, and F. Rompineve, *The Supercooled Universe*, JHEP **03** (2019) 100, [[arXiv:1812.06996](#)].
- [110] S. J. Lee, Y. Nakai, and M. Suzuki, *Multiple hierarchies from a warped extra dimension*, JHEP **02** (2022) 050, [[arXiv:2109.10938](#)].